PTEP

Prog. Theor. Exp. Phys. **2021**, 103B04 (47 pages)
DOI: 10.1093/ptep/ptab086

Quantum phase transition and resurgence: Lessons from three-dimensional $\mathcal{N} = 4$ supersymmetric quantum electrodynamics

Toshiaki Fujimori[1], Masazumi Honda[2], Syo Kamata[3], Tatsuhiro Misumi[1,4], Norisuke Sakai[1], and Takuya Yoda[5,*]

[1]*Department of Physics, and Research and Education Center for Natural Sciences, Keio University, 4-1-1 Hiyoshi, Yokohama, Kanagawa 223-8521, Japan*
[2]*Center for Gravitational Physics, Yukawa Institute for Theoretical Physics, Kyoto University, Sakyo-ku, Kyoto 606-8502, Japan*
[3]*National Centre for Nuclear Research, 02-093 Warsaw, Poland*
[4]*Department of Mathematical Science, Akita University, Akita 010-8502, Japan*
[5]*Department of Physics, Kyoto University, Kyoto 606-8502, Japan*
[*]E-mail: t.yoda@gauge.scphys.kyoto-u.ac.jp

Received March 29, 2021; Accepted June 23, 2021; Published July 14, 2021

We study a resurgence structure of a quantum field theory with a phase transition to uncover relations between resurgence and phase transitions. In particular, we focus on three-dimensional $\mathcal{N} = 4$ supersymmetric quantum electrodynamics (SQED) with multiple hypermultiplets, where a second-order quantum phase transition has recently been proposed in the large-flavor limit. We provide interpretations of the phase transition from the viewpoints of Lefschetz thimbles and resurgence. For this purpose, we study the Lefschetz thimble structure and properties of the large-flavor expansion for the partition function obtained by the supersymmetric localization. We show that the second-order phase transition is understood as a phenomenon where a Stokes and an anti-Stokes phenomenon occur simultaneously. The order of the phase transition is determined by how saddles collide at the critical point. In addition, the phase transition accompanies an infinite number of Stokes phenomena due to the supersymmetry. These features are appropriately mapped to the Borel plane structures as the resurgence theory expects. Given the lessons from SQED, we provide a more general discussion on the relationship between the resurgence and phase transitions. In particular, we show how the information on the phase transition is decoded from the Borel resummation technique.

Subject Index B14, B17, B34, B87

1. Introduction

One of the most important problems in quantum field theory (QFT) is to determine phase structures in the space of parameters. It is connected to significant information such as symmetries, energy gap, critical phenomena, topological order, etc. In particular, second-order phase transitions are essential as they often describe the starts and goals of renormalization group flows. It is natural to expect that phase transitions are technically related to (anti-)Stokes phenomena as they both describe some discontinuous behaviors of physical quantities in a certain limit of parameters. A well-known example of this is the connection between first-order phase transitions and anti-Stokes phenomena, as switches of dominant saddle points occur across anti-Stokes lines. However, the connections for higher-order cases are less clear, and it seems necessary to study them in a systematic framework. One such approach to describe Stokes phenomena is *resurgence theory* [1], which has recently attracted

Funded by SCOAP[3]

much attention in the context of QFTs.[1] This paper aims to study relations between phase transitions and resurgence in QFTs.

Resurgence theory has a long history of applications to quantum mechanics and differential equations. It has often been used to cure situations where perturbative expansions are not convergent. It typically gives relations between non-perturbative effects and large-order behaviors of perturbative series. There have been applications of resurgence to many physical systems, including quantum mechanics [7–36], hydrodynamics [37–44], integrable systems [45–52], non-critical string theory [53–57], and string theory [58–71], as well as QFTs. Recently there have also been various applications to QFTs, such as two-dimensional QFTs [72–88], the three-dimensional (3d) Chern–Simons theory [89–96] and Skyrme model [97], four-dimensional non-supersymmetric QFTs [98–108], and supersymmetric (SUSY) gauge theories in various dimensions [65,109–122].[2] However, most works have focused on systems without phase transitions, while we will mention some works related to phase transitions.

In this paper we study the resurgence structure of a QFT model with a phase transition to study the relations between resurgence and phase transitions. We take two approaches to address this problem. The first approach is Lefschetz thimble (steepest descents) analysis [9,10,130].[3] For a Lagrangian QFT, physical observables admit path integral representations and we can decompose them in terms of Lefschetz thimbles associated with saddle points in the field configuration space. In general, the structure of such a thimble decomposition can change discontinuously as parameters vary continuously in the theory under consideration. When this happens, asymptotic expansions around saddle points exhibit discontinuous changes of their forms, called Stokes phenomena. Other interesting phenomena related to thimble decomposition are anti-Stokes phenomena, where dominantly contributing saddles are switched as parameters vary while the thimble structures themselves are unchanged. As mentioned above, anti-Stokes phenomena typically induce a first-order phase transition which is often discussed in theoretical physics simply by comparing values of actions at saddle points. Here we mainly focus on relations between second-order phase transitions and Stokes phenomena. The other approach is to interpret from the viewpoint of Borel resummation. The information from such phenomena is expected to be encoded in a perturbative series. The Borel resummation technique enables us to decode such information. Therefore, if the resurgence theory works, then we can approach phase transitions (typically by non-perturbative effects) from perturbative expansions.

Here we mainly study three-dimensional $\mathcal{N} = 4$ supersymmetric quantum electrodynamics (SQED) with multiple hypermultiplets to obtain lessons on the relations between resurgence and phase transitions. It was recently proposed by Russo and Tierz [143] that there is a quantum second-order phase transition in SQED based on saddle point analysis in the large-flavor limit. They argued that the number of dominant saddle points changes across a particular value of the Fayet–Illiopoulos (FI) parameter and, assuming that they all contribute to the path integral, induces the phase transition. We provide interpretations of the phase transition from the viewpoints of Lefschetz thimbles and resurgence. We first justify the assumption in Ref. [143] that all the dominant complex saddles contribute to the path integral by Lefschetz thimble analysis. Then we interpret the second-order phase transition as simultaneous Stokes and anti-Stokes phenomena. Our results show that the resurgence

[1] See, e.g., the reviews in Refs. [2–6] for details.

[2] There are also studies on relations to renormalization [51,123–127], thermalization [128], and large charge expansions [129].

[3] See also Refs. [131–142].

theory works for describing the second-order phase transition of SQED. Given the lessons from SQED, we finally provide a more generic discussion on the relations between resurgence and phase transitions. In particular, we show generally that the orders of phase transitions are determined by how saddle points collide and scatter as a parameter varies through a critical point. We also show how information of the phase transition is decoded from the Borel resummation technique. We believe that our results open up potential applications of resurgence to quantum field theories.

Let us also comment on previous works closely related to this paper.[4] Reference [147] studied thimble structures of simple fermionic systems such as zero-dimensional versions of the Gross–Neveu model and Nambu–Jona-Lasinio model, and one-dimensional gauge theory coupled to a massive fermion with a Chern–Simons term. In particular, it was found in the zero-dimensional Gross–Neveu model that there was a jump in the number of contributing thimbles at the second-order chiral phase transition point in the massless case. An interesting link between anti-Stokes lines and Lee–Yang zeros was also demonstrated. There are also interesting works on the two-dimensional pure $U(N)$ Yang–Mills theory on the lattice [81,148,149], which is technically reduced to a unitary matrix model called the Gross–Witten–Wadia model [150,151].[5] It was found that a condensation of complex saddle points occurred at the third-order phase transition point in the large-N limit. Historically, physicists have studied simple models to draw lessons and to uncover general laws. The field of resurgence and its relation to QFT phase transitions is not an exception either. Now is a good time to broaden the reach of resurgence toward more realistic QFTs. The SQED studied in this paper should be a nice first step along this direction since it is more realistic; nevertheless, its partition function is expressed in a simple manner thanks to the supersymmetry.

This paper is organized as follows. In Sect. 2 we review the work by Russo and Tierz [143]. In Sect. 3 we provide interpretations of the phase transition from the viewpoint of Lefschetz thimbles. In Sect. 4 we discuss relations between the phase transition and resurgence structures. In Sect. 5, given the lessons from the SQED example, we give a more generic point of view on relations between the resurgence and phase transitions. Section 6 is devoted to conclusion and discussions. In App. A we explain details of the calculations of the $1/N_f$ flavor expansion, where $2N_f$ is the number of SQED hypermultiplets. In App. B we present thimble structures for larger $\arg(N_f)$, while the main text focuses around $\arg(N_f) = 0$. In App. C we make some comments on the Padé-Uniformized approximation based on comparisons with the standard Padé approximation in some simple examples. In Apps. D and E we study resurgence structures of the $1/N_f$ expansion from the viewpoint of a difference equation for finite values of the FI parameter η and the rescaled parameter $\lambda = \eta/N_f$, respectively. In App. F we point out a possible relation between the Borel singularities and complex supersymmetric solutions found in Ref. [115].

2. Quantum phase transition in the 3d $\mathcal{N} = 4$ SQED

In this section we review the arguments of Ref. [143] to find the quantum phase transition in 3d $\mathcal{N} = 4$ SQED with a large number of hypermultiplets. Let us consider a 3d $\mathcal{N} = 4$ SUSY $U(1)$ gauge theory coupled to $2N_f$ hypermultiplets with charge 1. We turn on an FI term and a real mass associated with a $U(1)$ subgroup of the $SU(2N_f)$ flavor symmetry.[6]

[4] See also Refs. [47–52,144–146] for works indirectly related to this context.

[5] The Painlevé equations were further studied in Refs. [152,153]

[6] The $U(1)$ subgroup rotates N_f hypermultiplets with charge $+1$ and the other N_f hypermultiplets with charge -1.

Applying the SUSY localization [154], the path integral is dominated by saddle points and one can exactly compute the S^3 partition function of this theory as [155–157]

$$Z = \int_{-\infty}^{\infty} d\sigma \frac{e^{i\eta\sigma}}{\left[2\cosh\frac{\sigma+m}{2}\cdot 2\cosh\frac{\sigma-m}{2}\right]^{N_f}}, \tag{2.1}$$

where η is the FI parameter and m is the real mass. The integral variable σ is the Coulomb branch parameter and the factor in the denominator is the one-loop determinant of the hypermultiplets.[7]

Now we are interested in the 't Hooft-like limit:

$$N_f \to \infty, \qquad \lambda \equiv \frac{\eta}{N_f} = \text{fixed}. \tag{2.2}$$

For this purpose, it is convenient to write the partition function as

$$Z = \frac{1}{2^{N_f}} \int_{-\infty}^{\infty} d\sigma\, e^{-S(\sigma)}, \tag{2.3}$$

where $S(\sigma)$ is the "action" defined by

$$S(\sigma) = N_f\Big[-i\lambda\sigma + \ln(\cosh\sigma + \cosh m)\Big]. \tag{2.4}$$

In the large-N_f limit, the integral is dominated by saddle points satisfying

$$S'(\sigma) = N_f\left(-i\lambda + \frac{\sinh\sigma}{\cosh\sigma + \cosh m}\right) = 0. \tag{2.5}$$

This equation is solved by

$$\sigma_n^{\pm} = \log\left(\frac{-\lambda\cosh m \pm i\Delta(\lambda, m)}{i+\lambda}\right) + 2\pi i n \qquad (n \in \mathbb{Z}), \tag{2.6}$$

where

$$\Delta(\lambda, m) = \sqrt{1 - \lambda^2\sinh^2 m}. \tag{2.7}$$

The action at the nth saddle point is

$$S(\sigma_n^{\pm}) = N_f\left[-\frac{i\lambda}{2}\ln\left(\frac{-i+\lambda}{i+\lambda}\frac{-\lambda\cosh m \pm i\Delta}{-\lambda\cosh m \mp i\Delta}\right) + \ln\left(\frac{\cosh m \pm \Delta}{1+\lambda^2}\right) + 2\pi n\lambda\right]. \tag{2.8}$$

Note that the saddles and the action values are complex in general. Also, note that the action can be written as

$$S(\sigma_n^{\pm}) = S(\sigma_0^{\pm}) + 2\pi n N_f \lambda. \tag{2.9}$$

[7] The integral in Eq. (2.1) can be solved exactly as

$$Z = \frac{\sqrt{2\pi}}{2^{N_f}} \frac{\Gamma(N_f + i\eta)\Gamma(N_f - i\eta)}{\Gamma(N_f)\,(\sinh m)^{N_f - 1/2}} P^{\frac{1}{2}-N_f}_{-\frac{1}{2}+i\eta}(\cosh m)$$

with the associated Legendre polynomial $P^m_\ell(x)$ [143], but this form does not seem particularly useful for our purpose.

This implies that the most dominant saddle point for real λ is either $\sigma = \sigma_0^+$ or $\sigma = \sigma_0^-$, if it contributes to the integral.

The authors of Ref. [143] observed that dominant saddles change at $\lambda = \lambda_c$, with

$$\lambda_c \equiv \frac{1}{\sinh m}. \tag{2.10}$$

For the subcritical region $\lambda < \lambda_c$, only a single saddle, σ_0^+, dominates the integral. For the supercritical region $\lambda \geq \lambda_c$, two saddles, σ_0^+ and σ_0^-, contribute to the integral with equal weights. Reference [143] numerically checked that these saddle approximations agree with the exact analytic expression of Eq. (2.1) at the large-N_f limit. The second derivative of the "free energy" jumps at $\lambda = \lambda_c$ as

$$\frac{d^2F}{d\lambda^2} = \begin{cases} \frac{N_f}{1+\lambda^2}\left(1 + \frac{\cosh m}{\sqrt{1-\lambda^2\sinh^2 m}}\right) & \lambda < \lambda_c, \\ \frac{N_f}{1+\lambda^2} & \lambda \geq \lambda_c. \end{cases} \tag{2.11}$$

This implies that the system exhibits a second-order phase transition at $\lambda = \lambda_c$.

3. Lefschetz thimble structures

In general, saddles with smaller $\Re S$ give larger weights. However, such saddles do not necessarily contribute to the path integral. This is because the original integration contour may not be deformed to the Lefschetz thimbles (steepest descent paths) associated with such saddles. Also note that the "free energy" of a partition function on a general manifold is not necessarily real since it is not interpreted as a thermodynamic one. This means that contributing saddles cannot be determined only by requiring the free energy to be real. For these reasons, we should study Lefschetz thimble structures to describe quantum phase transitions.

In this section we interpret the quantum phase transition in terms of Lefschetz thimbles of the integral in Eq. (2.1) obtained by SUSY localization. This provides a more precise justification for the arguments in Ref. [143] reviewed in the previous section. For this purpose, we first extend the Coulomb branch parameter $\sigma \in \mathbb{R}$ to complex values $z \in \mathbb{C}$, since saddle points and the associated Lefschetz thimbles are complex-valued in general. As we saw in the last section, we have infinitely many saddle points $\sigma_n^\pm$ satisfying the saddle point equation. Contributing saddles are determined by looking at the Lefschetz thimbles (or the steepest descents) obtained by deforming the original contour without changing the value of the integral. This can depend on the original integral contour, the parameters (λ, m) and properties of the (dual) Lefschetz thimbles as explained below.

The Lefschetz thimbles $\mathcal{J}_n^\pm$ associated with the saddle points $\sigma_n^\pm$ are defined as solutions of the differential equation called the flow equation,

$$\left.\frac{dz}{ds}\right|_{\mathcal{J}_n^\pm} = \overline{\frac{\partial S[z]}{\partial z}}, \tag{3.1}$$

with the initial conditions

$$\lim_{s\to-\infty} z(s) = \sigma_n^\pm, \tag{3.2}$$

where s is the flow parameter along the Lefschetz thimbles. Using the flow equation, we can easily prove the following properties:

$$\left.\frac{d}{ds}\mathrm{Re}S[z(s)]\right|_{\mathcal{J}_n^\pm} \geq 0, \qquad \left.\frac{d}{ds}\mathrm{Im}S[z(s)]\right|_{\mathcal{J}_n^\pm} = 0. \tag{3.3}$$

These indicate that integrals along Lefschetz thimbles are rapidly convergent and non-oscillating. We can express the original contour $\mathcal{C}_\mathbb{R}$ as a linear combination of Lefschetz thimbles:

$$\mathcal{C}_\mathbb{R} = \sum_\pm \sum_{n=-\infty}^{\infty} k_n^\pm \mathcal{J}_n^\pm. \tag{3.4}$$

If $k_n^\pm$ is nonzero, it implies that $\sigma_n^\pm$ contributes to the integral while we have no contributions from the saddle points with $k_n^\pm = 0$. It is known that each expansion coefficient $k_n^\pm$ is an integer since $k_n^\pm$ is identified with the intersection number between the original contour $\mathcal{C}_\mathbb{R}$ and the dual thimble (or the steepest ascent contour) $\mathcal{K}_n^\pm$ associated with $\sigma_n^\pm$, which is defined by

$$\left.\frac{dz}{ds}\right|_{\mathcal{K}_n^\pm} = \overline{\frac{\partial S[z]}{\partial z}}, \qquad \lim_{s\to+\infty} z(s) = \sigma_n^\pm. \tag{3.5}$$

In general, $k_n^\pm$ depends on (g, m) but its dependence is not continuous since $k_n^\pm$ is an integer. Typically $k_n^\pm$ is a constant or a step function, and the latter case leads us to a Stokes phenomenon.

3.1. Real positive N_f

First, let us briefly see the Lefschetz thimble structures for real positive N_f, i.e. $\arg(N_f) = 0$. We have numerically solved the flow equations and show the results at some representative values of (m, λ) in Fig. 1. We immediately see that the Lefschetz thimbles pass multiple saddle points in both the subcritical ($\lambda < \lambda_\mathrm{c}$) and supercritical ($\lambda \geq \lambda_\mathrm{c}$) regions. Although we have explicitly shown the results only at two values of (m, λ), we have checked that this feature holds unless the parameters cross the phase boundary. The thimble structures imply that the decomposition in terms of the thimbles is not well defined at $\arg(N_f) = 0$ and the Stokes coefficient has a discrete change. In other words, the present case $\arg(N_f) = 0$ is on Stokes lines.

The appearance of the Stokes lines here is natural because we have infinitely many saddle points with the same imaginary part of the action at $\arg(N_f) = 0$, although this is not sufficient but necessary to get the Stokes lines. This can be explicitly seen as follows. In the subcritical region $\lambda < \lambda_\mathrm{c}$, one can easily show that all the saddle points are purely imaginary and their actions are real:

$$\mathrm{Im}(S_n^\pm) = 0 \quad \text{for} \quad \lambda < \lambda_\mathrm{c}. \tag{3.6}$$

In the supercritical region $\lambda > \lambda_\mathrm{c}$, the imaginary parts of the actions at the saddles are nonzero but they satisfy

$$\mathrm{Im}(S_n^\pm) = -\mathrm{Im}(S_n^\mp), \qquad \mathrm{Im}(S_n^\pm) = \mathrm{Im}(S_0^\pm), \qquad \text{for all } n \text{ and } \lambda > \lambda_\mathrm{c}. \tag{3.7}$$

The above structure essentially comes from the fact that the action at the saddles depends on n only via the term $2\pi n\lambda N_f$, as seen from Eq. (2.9). This motivates us to take complex N_f to go beyond the Stokes lines and understand the thimble structures more precisely.

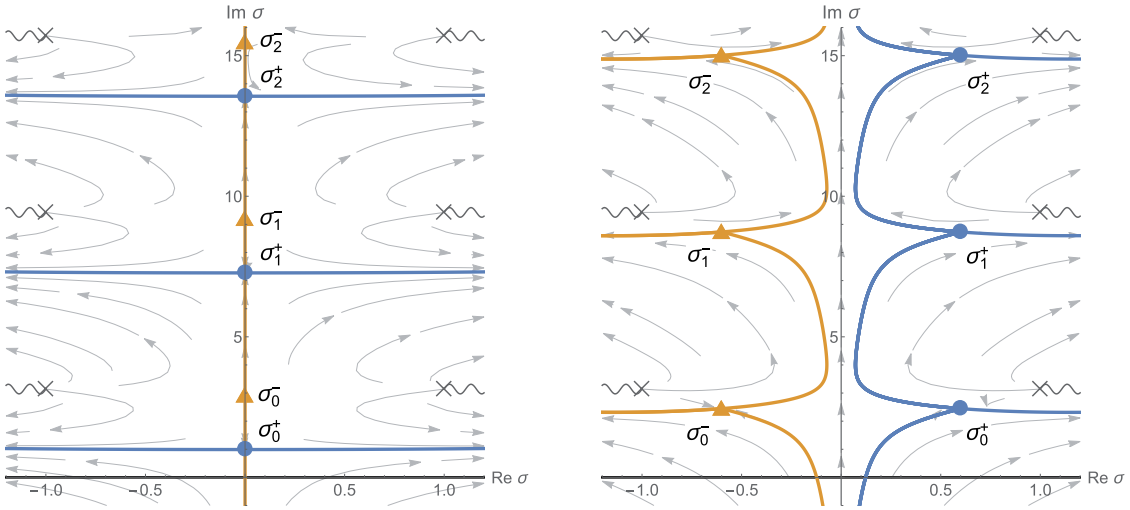

Fig. 1. Illustrations of the Lefschetz thimble structures of the integral in Eq. (2.1) for $\arg(N_f) = 0$. (In these figures, $m = 1$, for which $\lambda_c \simeq 0.85$). The blue circle and orange triangle symbols indicate the saddles σ_n^+ and σ_n^-, respectively. The Lefschetz thimbles associated with them are drawn as lines with the same colors. The gray wavy lines and cross symbols indicate the branch cuts and singularities of the action in Eq. (2.4), which essentially come from the logarithm. Left: At $\lambda = 0.4 < \lambda_c$ as a representative of the subcritical region. Right: At $\lambda = 1.2 > \lambda_c$ as a representative of the supercritical region.

3.2. *Complex N_f*

Let us take N_f to be complex while keeping λ real,[8]

$$\theta \equiv \arg(N_f), \tag{3.8}$$

and study the Lefschetz thimble structures. In the main text we study the thimble structures only around $\theta = 0$. See App. B for the non-small-θ case.

Let us first focus on the subcritical region $\lambda < \lambda_c$ presented in Fig. 2. Regardless of the sign of θ, the dual thimble $\mathcal{K}_0^+$ intersects once with the original integration contour $\mathcal{C}_\mathbb{R}$. This means that the original integral contour $\mathcal{C}_\mathbb{R}$ can be deformed to the thimble $\mathcal{J}_0^+$. Indeed, we can apply Cauchy's integral formula since the integrand decreases at infinity on the upper-half plane. Thus, we find a unique thimble decomposition

$$\mathcal{C}_\mathbb{R} = k_0^+ \mathcal{J}_0^+, \qquad k_0^+ = 1. \tag{3.9}$$

In other words, there is no Stokes phenomenon in the subcritical region.

The structures in the supercritical region $\lambda > \lambda_c$ are shown in Fig. 3. We observe qualitatively different behaviors compared with the subcritical region.[9] Firstly, multiple saddle points contribute to the integral. In particular, two saddle points $\sigma_0^\pm$ always contribute as their dual thimbles always intersect with the original integral contour $\mathcal{C}_\mathbb{R}$. This justifies the arguments in Ref. [143] reviewed in Sect. 2. Note that this fact is a priori nontrivial since the saddles are complex. Secondly, the intersection numbers $k_{n\geq 1}^\pm$ jump discontinuously as the phase θ is changed. The thimble structures depend not only on the sign of θ but also on the absolute value $|\theta|$. Specifically, a common feature for each sign $\pm$ of $\sigma_n^\pm$ is that the saddle points $\sigma_{n\geq 1}^\pm$ do not contribute for $\text{sign}(\theta) = \mp$. The dependence

[8] To keep λ real, we should also take $\arg(\eta) = \theta$ since $\lambda = \eta/N_f$.

[9] It is common that the saddle points $\sigma_n^\pm$ with $n < 0$ never contribute.

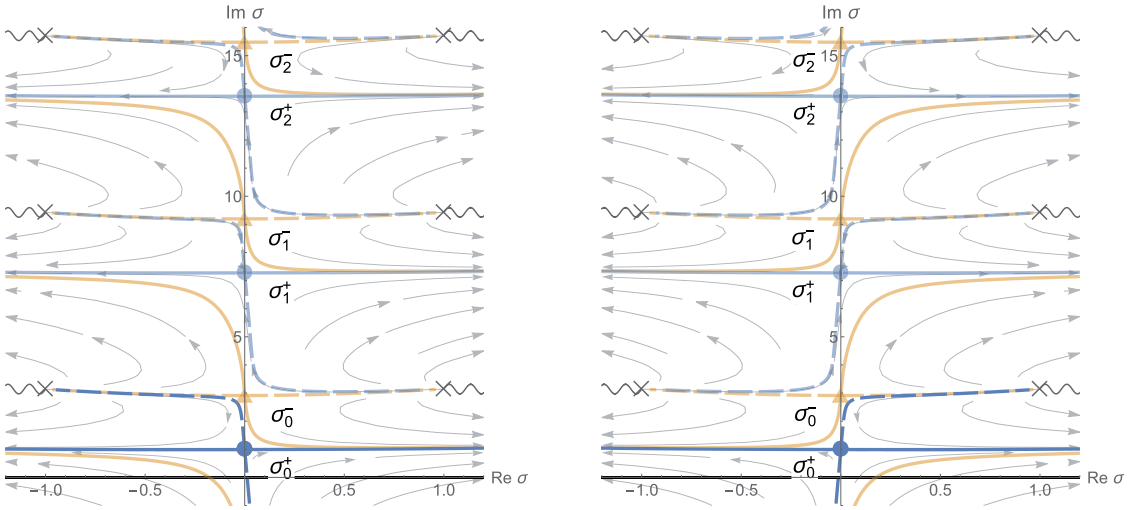

Fig. 2. Illustrations of the Lefschetz thimble structure for the subcritical region $\lambda = 0.4 < \lambda_c$ with $m = 1$. Small phases $\theta = -0.025$ (left) and $\theta = +0.025$ (right) are given to illustrate behaviors around $\theta = 0$. The solid lines show the Lefschetz thimbles, while the dashed lines are the dual thimbles associated with saddle points. The opaque saddles and thimbles contribute to the integral, while the translucent ones do not. In this case, the contributing saddle σ_0^+ does not change for any small θ.

on the absolute value $|\theta|$ is more intricate. At $\theta = +0.025$, shown at the top right of Fig. 3, we see that σ_1^+ contributes while σ_n^+ with $n \geq 2$ do not contribute. Similarly, at $\theta = +0.015$, shown at the bottom right of Fig. 3, we see that σ_1^+ and σ_2^+ contribute but σ_n^+ with $n \geq 3$ do not contribute. As we further decrease $|\theta|$, we find the following structure (although we do not explicitly show the plots). For finite $\theta > 0$ ($\theta < 0$), we have contributions from the saddle points σ_n^+ with $1 \leq n \leq M_+(\theta)$ (σ_n^- with $1 \leq n \leq M_-(\theta)$), where $M_\pm(\theta)$ is an integer such that

$$M_\pm(\theta) \to \infty \quad \text{as} \quad \theta \to \pm 0. \tag{3.10}$$

In summary, the above analysis suggests the following thimble structure in the supercritical region:

$$\mathcal{C}_{\mathbb{R}} = k_0^+ \mathcal{J}_0^+ + k_0^- \mathcal{J}_0^- + \sum_{\pm, n \geq 1} k_n^\pm \mathcal{J}_n^\pm, \tag{3.11}$$

where

$$k_0^+ = k_0^- = 1, \qquad k_{n\geq 1}^+ = \begin{cases} 0 & (\theta = -0) \\ 1 & (\theta = +0) \end{cases}, \qquad k_n^- = \begin{cases} 1 & (\theta = -0) \\ 0 & (\theta = +0) \end{cases}. \tag{3.12}$$

This indicates an infinite number of Stokes phenomena at $\theta = 0$ in the supercritical region.

3.3. *Phase transition and thimble structures*

We clarify the relation between the phase transition and the above Lefschetz thimble analysis. Whether the saddles contribute to the integral was a priori nontrivial since all of them are complex for $\lambda > 0$. Our Lefschetz thimble analysis showed that only a single saddle σ_0^+ contributes to the integral in the subcritical region $\lambda < \lambda_c$, while multiple saddles $\sigma_n^\pm$ with $n \geq 0$ contribute in the supercritical region $\lambda \geq \lambda_c$. Among them, only two saddles $\sigma_0^\pm$ survive the large-flavor limit. Thus, the dominant saddles jump at the critical point $\lambda = \lambda_c$ from σ_0^+ to $\sigma_0^\pm$, which causes the phase transition. These provide a more precise interpretation of the phase transition in terms of the

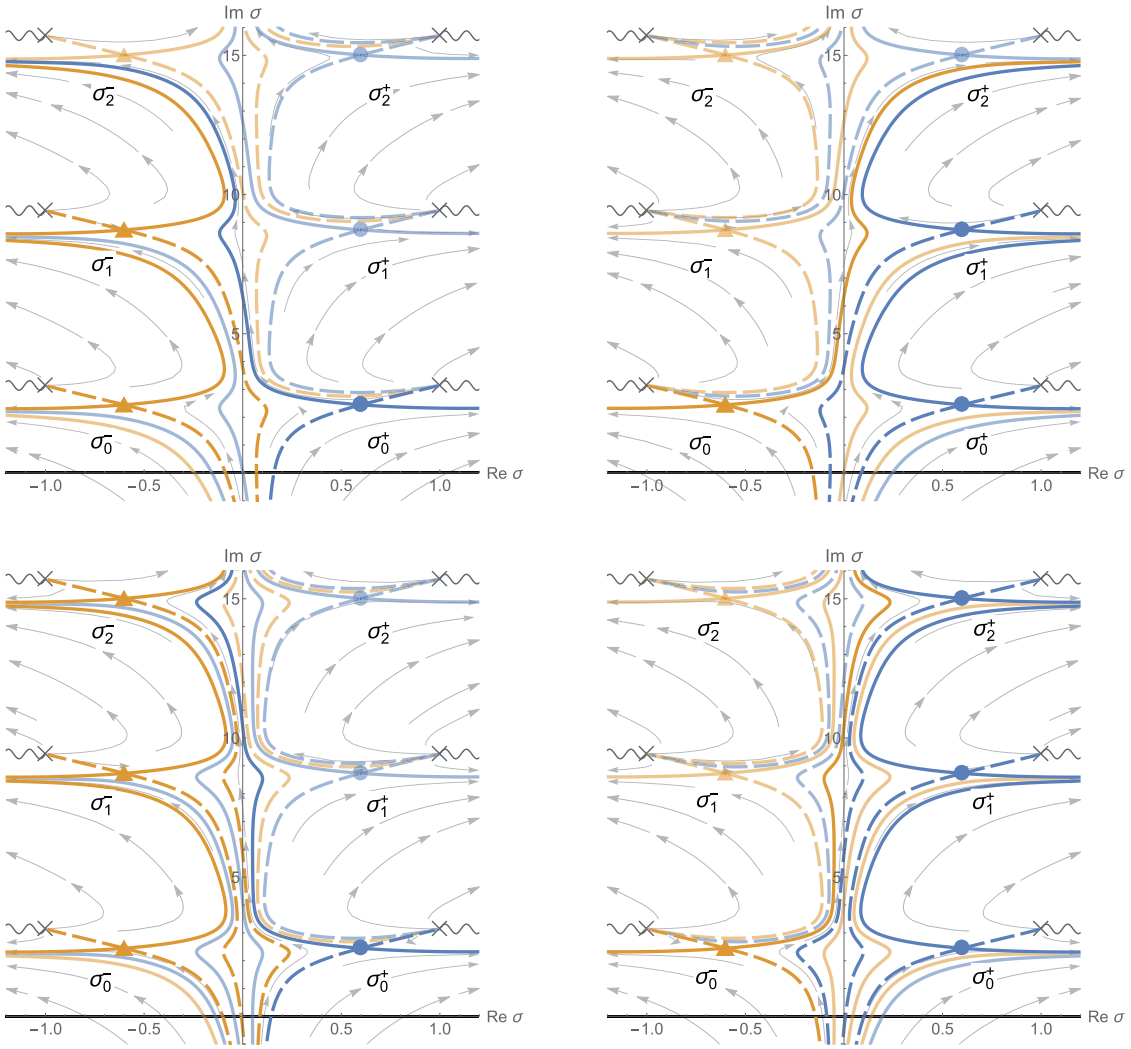

Fig. 3. Illustrations of the thimble structure for the supercritical region $\lambda = 1.2 > \lambda_c$ with $m = 1$. Small phases $\theta = -0.025$ (top left), $\theta = +0.025$ (top right), $\theta = -0.015$ (bottom left), and $\theta = +0.015$ (bottom right) are given to illustrate behaviors around $\theta = 0$. Contrary to the subcritical region, the contributing saddles change discontinuously. As the phase approaches $\theta \to \pm 0$, saddle points $\sigma_n^{\pm}$ with larger n contribute to the path integral.

Lefschetz thimble analysis. All of these behaviors come from (anti-)Stokes phenomena and therefore these motivate us to study, in more detail, the relation between the phase transition and (anti-)Stokes phenomena. This will be summarized in Sect. 5.

Also, note that the periodicity of the action in Eq. (2.4) along the imaginary axis causes an infinite number of Stokes phenomena at $\arg(N_f) = 0$. Such a property is typical in sphere partition functions of $\mathcal{N} \geq 4$ supersymmetric gauge theories with FI terms and without diagonal Chern–Simons terms. This infinite number of Stokes phenomena are inevitably related to the phase transition, as we will see in more detail in Sect. 5.

Finally, we briefly provide some preparation for the next section. We have collected the thimble structures for larger values of $\arg(N_f)$, as summarized in App. B. For non-small $\arg(N_f)$, we have encountered a subtlety essentially coming from the logarithmic branch cuts in the action of Eq. (2.4): when a thimble crosses the branch cuts once, the action changes its value by $\pm 2\pi i N_f$, where the

sign depends on the direction of the crossing. Note that this modifies the condition for having Stokes phenomena as the imaginary part of the action is changed. Appendix B demonstrates that the Stokes phenomena due to this effect indeed happen in our problem. For instance, in the subcritical region $(\lambda, m) = (0.4, 1)$ we found numerically that the Lefschetz thimble associated with the saddle σ_0^+ crosses one of the branch cuts once and then passes the neighboring saddle σ_1^+ around $\arg(N_f) \simeq -1.190$. The appearance of this Stokes phenomenon cannot be understood without taking the effect of the branch cuts into account as follows. The existence of the branch cut implies that the condition for having Stokes phenomena between the saddles σ_n^+ and σ_0^+ is modified as

$$\Im\left[S(\sigma_n^+) - S(\sigma_0^+) + 2\pi i N_f \mathbb{Z}\right] = 0, \tag{3.13}$$

which is solved by

$$\tan\theta = -\frac{1}{n\lambda}\mathbb{Z}. \tag{3.14}$$

This condition specifically for the above case corresponds to $\theta = \arctan(-1/\lambda)|_{\lambda=0.4} \simeq -1.190$, which agrees with the result in App. B. Similarly, in the supercritical region $(\lambda, m) = (1.2, 1)$ we found the Stokes phenomenon between σ_1^- and σ_0^+ coming from the effect of the branch cuts for $\theta \simeq= -0.039$.

From the viewpoint of the resurgence theory, the information of Stokes phenomena is encoded in the $1/N_f$ expansion of the partition function in Eq. (2.1). The Stokes phenomena observed in the figures in App. B are associated with the Borel singularities of the $1/N_f$ expansion. Relations between Stokes phenomena and Borel singularities in one-dimensional integrals are shown in Refs. [158–160], although some of the assumptions there are violated in SQED due to the logarithmic branch cuts in the action. We will discuss corresponding Borel singularities in the next section.

4. Borel singularities and resurgence structure

In this section we consider the $1/N_f$ expansion of the partition function in Eq. (2.1) and study its resurgence structure from the viewpoint of the Borel resummation method. We numerically compute the $1/N_f$ expansion up to 50th order and then study the structures of the Borel singularities. We confirm that the locations of the Borel singularities are consistent with the Lefschetz thimble structure. The resurgence structure of trans-series with respect to η or λ, instead of $1/N_f$, is discussed in Apps. D and E.

4.1. Numerical study of Borel singularities

Let us focus on the $1/N_f$ expansion around the saddle point $\sigma = \sigma_0^+$. It can be computed in the standard way and the expansion takes the form (see App. A for details)

$$\int_{\mathcal{J}_0^+} d\sigma\, e^{-N_f \tilde{S}(\sigma)} = e^{-N_f \tilde{S}(\sigma_0^+)} \sqrt{\frac{2\pi}{N_f \tilde{S}''(\sigma_0^+)}} \sum_{\ell=0}^{\infty} \frac{a_\ell}{N_f^\ell}, \tag{4.1}$$

where

$$S(\sigma) = N_f \tilde{S}(\sigma). \tag{4.2}$$

The coefficients are given by

$$a_\ell = \sum_{n=0}^{2\ell} \frac{(-1)^n \Gamma\left(\frac{1}{2}+\ell+n\right) \tilde{c}_{2\ell-n}(n)}{\Gamma(1/2)\Gamma(n+1)}, \tag{4.3}$$

where

$$\tilde{c}_k(n) = \left(\sum_{k'=0}^{\infty} c_{k'} \epsilon^{k'} \right)^n \Bigg|_{\epsilon^k}, \qquad c_k = \frac{2^{\frac{k+3}{2}}}{(k+3)!} \frac{\tilde{S}^{(k+3)}(\sigma_0^+)}{\left(\tilde{S}''(\sigma_0^+)\right)^{\frac{k+3}{2}}}. \tag{4.4}$$

This implies that the coefficient a_ℓ grows factorially and the formal $1/N_f$ expansion is not convergent. We therefore apply the Borel resummation technique to control the divergence. Let us write the perturbation series as

$$F\left(\frac{1}{N_f}\right) = \sum_{\ell=0}^{\infty} \frac{a_l}{N_f^\ell}, \tag{4.5}$$

and define its Borel transformation by

$$\mathcal{B}F(t) = \sum_{l=0}^{\infty} \frac{a_\ell}{\Gamma(\ell+1)} t^\ell = \sum_{\ell=0}^{\infty} b_\ell t^\ell. \tag{4.6}$$

Then, the Borel resummation of the function $F(1/N_f)$ is given by

$$F_C\left(\frac{1}{N_f}\right) = N_f \int_C dt\, e^{-N_f t} \widetilde{\mathcal{B}F}(t), \tag{4.7}$$

where $\widetilde{\mathcal{B}F}(t)$ is a simple analytic continuation of the series in Eq. (4.6) and the integration contour C is chosen so that $\arg(N_f t) = 0$. The Borel resummation discontinuously changes if the integration contour crosses a singularity of $\mathcal{B}F(t)$. From the viewpoint of resurgence, the Borel singularities must correspond to Stokes phenomena summarized in App. B.

4.1.1. The Padé approximation and its improvement

As seen from Eq. (4.6), the Borel transformation is defined in terms of an infinite number of the perturbative coefficients. In practice, we often encounter the situation where we know only a finite number of the coefficients and have to estimate (the analytic continuation of) the Borel transformation from the limited perturbative data in some way. One of the standard ways to do this is the so-called Borel–Padé approximation, where we replace the Borel transformation $\widetilde{\mathcal{B}F}(t)$ in Eq. (4.7) by its Padé approximation. The Padé approximation with degrees (m, n) is defined by a rational function,

$$\mathcal{P}_{m,n}(t) = \frac{P_m(t)}{Q_n(t)}, \tag{4.8}$$

where $P_m(t)$ and $Q_n(t)$ are polynomials of degrees m and n, respectively. The explicit forms of the polynomials are determined such that the small-t expansion of $\mathcal{P}_{m,n}(t)$ agrees with the Borel transformation up to a desired order L:

$$\sum_{\ell=0}^{L} b_\ell t^\ell = \mathcal{P}_{m,n}(t) + \mathcal{O}(t^{L+1}), \qquad m+n=L. \tag{4.9}$$

While there are various possible choices of (m, n) given L, it is empirically known that the Padé approximation often has better accuracy when m and n are close. Therefore, here we take $m = n = L/2$ with even L and do not pursue (m, n) dependence. This particular case is called the diagonal Padé approximation. In practice, we will present results for $L = 50$ as representative.

In general, the Padé approximation is good at approximating meromorphic functions since it has only pole-type singularities. For cases with branch cuts, the Padé approximation typically becomes worse as it is impossible to express branch cuts in terms of a rational function in the exact sense. It is known that when the Padé approximation works for the cases with branch cuts, sets of dense poles appear around the locations of the branch cuts.[10] It is also known that the Padé approximation generically gives better descriptions for singularities closer to the origin $t = 0$. In particular, the location of the closest singularity is expected to be predicted when (m, n) is larger because this information is closely related to the radius of the convergence of the small-t expansion. In other words, it is typically hard to detect Borel singularities far away from the origin when (m, n) is not so large.

There are various ways to improve the Padé approximation in Eq. (4.8). Here we use one of the improvements called the Padé-Uniformized approximation [161], which can be used when we know information on the location of a branch cut in the Borel transformation $\widetilde{\mathcal{B}F}(t)$. This is constructed as follows.[11] Suppose that the function $\widetilde{\mathcal{B}F}(t)$ has a branch cut ending at $t = s$. We send the Borel t-plane to a u-plane by the uniformization map

$$t \mapsto u(t) = -\ln\left(1 - \frac{t}{s}\right), \tag{4.10}$$

which can be inverted as

$$u \mapsto t(u) = s(1 - e^{-u}). \tag{4.11}$$

Note that the singularity at $t = s$ in the t-plane is mapped to infinity in the u-plane. Then we construct the standard Padé approximation in the u-plane, meaning that we construct a rational approximation $\mathcal{P}_{m,n}(u)$ such that

$$\mathcal{P}_{m,n}(u) = \sum_{\ell=0}^{L} b'_\ell u^\ell + \mathcal{O}(u^{L+1}), \qquad m + n = L, \tag{4.12}$$

where the coefficient b'_ℓ is defined to satisfy

$$\sum_{\ell=0}^{L} b'_\ell u^\ell = \sum_{\ell=0}^{L} b_\ell \left(t(u)\right)^\ell + \mathcal{O}(t^{L+1}). \tag{4.13}$$

Finally, we come back to the t-plane and approximate the Borel transformation as

$$\widetilde{\mathcal{B}F}(t) \simeq \mathcal{P}_{m,n}(u(t)). \tag{4.14}$$

[10] In other words, many poles in the Padé approximation are consumed to resemble the jump around the branch cuts, and we typically need larger (m, n).

[11] Another way to treat branch cuts is to use functions with branch cuts for approximation (e.g. fractional power of some simple functions). See Refs. [162–167] for such approaches.

The uniformization map sends the branch cut singularity to infinity, where the standard Padé approximation does not see it. Instead, it sends a region away from the branch cut singularity to a region around the origin. Thus, we can avoid pole resources of the Padé approximation being wasted on the branch cut. Also, thanks to the logarithm of the uniformization map, the order of Borel singularities affects only the scale of u. For example, $1/(1-t)^{1/n}$ is mapped just to $e^{u/n}$ and logarithmic singularities are mapped to regular points. Another good example is $\ln(1-t)$, which is simply mapped to $-u$. For the above reasons, the Padé-Uniformized approximation is safer than the standard Padé approximation in our particular application.

4.1.2. Subcritical region

Let us focus on the subcritical region $\lambda < \lambda_c$. In the left panel of Fig. 4 we present the locations of poles of the standard Padé approximation for the Borel transformation $\widetilde{\mathcal{B}F}(t)$, which is expected to approximate the Borel singularities. The red crosses indicate the poles of the Padé approximant while the other symbols denote the values of the saddle point actions subtracted by the values of σ_0^+ and their counterparts on different Riemann sheets.[12] The colored symbols among them denote the saddles at which Stokes phenomena are expected to occur from the Lefschetz thimble analysis in the previous section. In other words, a symbol associated with a saddle $\sigma_n^\pm$ is colored if there exists $\arg(N_f)$ such that[13]

$$\Im[S(\sigma_n^\pm) - S(\sigma_0^+) + 2\pi i N_f \mathbb{Z}] = 0. \tag{4.15}$$

From the viewpoint of resurgence, we expect that the Borel singularities are located at these color symbols.

In the left panel of Fig. 4 we see a bunching of poles around the point corresponding to the saddle σ_0^- and stretched along the negative real axis. According to general expectation on the Padé approximation, this signals that the Borel transformation has a branch-cut-type singularity ending on the point corresponding to σ_0^- along the negative real axis. This is consistent with the expectation that we have Stokes phenomena with σ_0^-. We also see good agreement between the locations of the poles and the action values at $N_f t = S(\sigma_1^+) \pm 2\pi i - S(\sigma_0^+)$ as expected from the thimble analysis. However, it seems that we do not have a similar agreement for the other saddles, in particular when we go away from the origin. One reason is that the Padé approximation becomes worse outside the convergence radius. Another reason is that there is a branch cut on the Borel t-plane. The Padé approximant has limited pole resources to resemble the genuine Borel plane structure. In our case there are only $L/2 = 25$ poles. If there is a branch cut, a lot of poles are consumed to resemble it. Indeed, a lot of poles are accumulated on the negative real axis. Thus, it seems more appropriate to use the Padé-Uniformized approximation using the input that we have a branch cut ending on the point $N_f t = S(\sigma_0^-) \pm 2\pi i - S(\sigma_0^+)$.

In the right panel of Fig. 4 we show the result of the Padé-Uniformized approximation where we have eliminated the expected branch cut by the uniformization map in EQ. (4.10). We first see that

[12] Recall the arguments at the end of Sect. 3.3. The thimble structures for non-small $\arg(N_f)$ studied in App. B imply that we have to take care of situations where thimbles cross the branch cuts and then the action is shifted by $2\pi i N_f \mathbb{Z}$.

[13] For example, as discussed at the end of Sect. 3.3 and demonstrated in App. B, this condition for $(\lambda, m) = (0.4, 1)$ is satisfied when $\arg(N_f) = -1.190$. Therefore, the circles on the ray $\arg(t) = -\arg(N_f) = 1.190$ are colored.

Fig. 4. Illustrations of the Borel plane structure for the subcritical region $\lambda = 0.4 < \lambda_c$ obtained by the standard Padé approximation (left panel) and the Padé-Uniformized approximation (right panel). The red cross symbols indicate the locations of poles found by the approximations. The circle/triangle symbols on the real axis indicate the values of the saddle point actions relative to the action of σ_0^+, which are specifically $N_f t = S(\sigma_n^\pm) - S(\sigma_0^+)$. The same symbols beyond the real axis are their counterparts on different Riemann sheets obtained by shifting those on the real axis by $2\pi i\mathbb{Z}$. The colored symbols among them denote the saddles at which Stokes phenomena are expected to occur from the Lefschetz thimble analysis.

there is no longer a bunching of dense poles as appeared in the standard Padé approximant. This confirms that the uniformization map has successfully removed the branch cut. Because of this, we expect that the Padé-Uniformized approximation gives a better description of other singularities. Indeed, the result shows better agreement between the locations of poles and the expected Borel singularities around the origin. In particular, note that there is no Borel singularity on the positive real axis. This is consistent with the Lefschetz thimble structure around $\arg(N_f) = 0$ as shown in Fig. 1. However, we see some poles around the real axis which do not coincide with action values. It seems that they are artifacts of the Padé approximation; for details, see App. C.

4.1.3. Supercritical region

The results for the supercritical region $\lambda \geq \lambda_c$ are shown in Fig. 5. As in the subcritical case, the left panels are the result of the standard Padé approximation while the right panels denote the Padé-Uniformized approximation. The upper and lower panels are essentially the same but we plot them at different scales for convenience. Note that the actions of the saddles σ_n^+ and σ_n^- are different by purely imaginary values even on the same Riemann surface.

Let us first focus on the result of the standard Padé approximation shown in the left panels of Fig. 5. We easily see that there is again a bunching of poles around the point corresponding to the saddle σ_0^-, but now they are stretched along the upper imaginary axis in contrast to the subcritical case. This again implies that the Borel transformation has a branch cut ending on the point corresponding to σ_0^- along the upper imaginary axis. While this agrees with the expectation from the resurgence, we do not see good agreement beyond that saddle. Therefore, we again improve the Padé approximation assuming the information on the branch cut as in the subcritical region.

The right panels of Fig. 5 show the result of the Padé-Uniformized approximation. The expected branch cut has been eliminated by the uniformization map in Eq. (4.10) and one can check that the

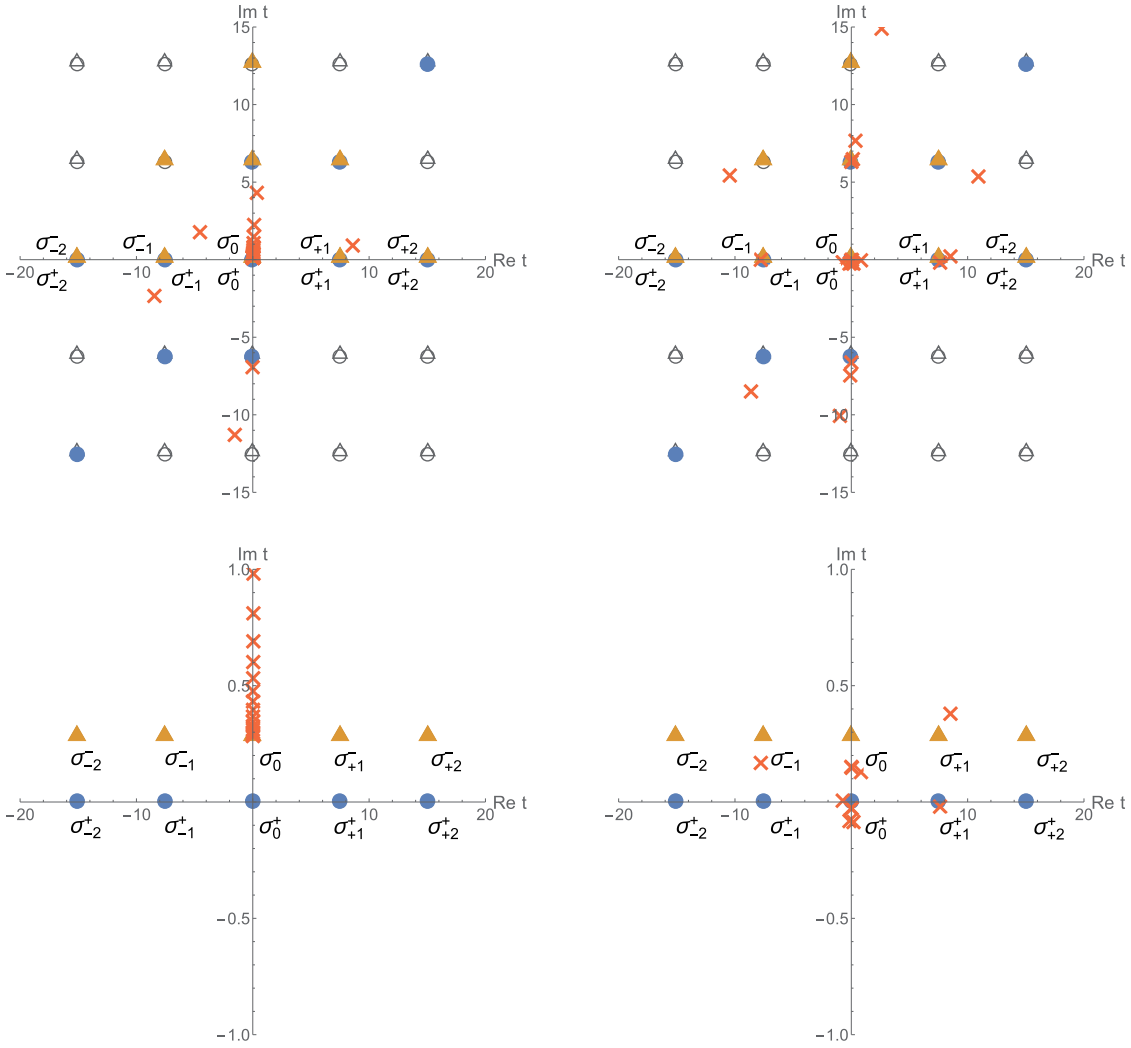

Fig. 5. Illustrations of the Borel plane structure for the supercritical region $\lambda = 1.2 > \lambda_c$ obtained by the Padé approximation (left panels) and the Padé-Uniformized approximation (right panels). The lower panels are zoomed versions of the upper ones.

bunching of dense poles is indeed absent in this case. We now see better agreement: there are poles around the expected locations of the Borel singularities. This is consistent with the Lefschetz thimble structure around $\arg(N_f) = 0$ as shown Fig. 2. However, we still have missing singularities away from the origin. For details, see App. C.

4.2. Analytical study of Borel singularities for large λ

In Sect. 4.1 we numerically found the Borel singularities at $2\pi i\mathbb{Z}$ in the supercritical region, as demonstrated in the right panel of Fig. 5. We infer this class of singularities corresponds to the saddle σ_0^+ on different Riemann sheets. Here we provide an analytical justification for that. We analytically prove that the Borel transformation of the $1/N_f$ expansion around the saddle point $\sigma_n^\pm$ has singularities at $2\pi i\mathbb{Z}$ in the large-λ limit.

Let us consider the large-λ limit $\lambda \gg \lambda_c$ and $\lambda \gg 1$. The saddle point $\sigma_n^\pm$ in this limit is expanded as

$$\sigma_{\pm}^{n} = \mp m + (2n+1)\pi i + \frac{i}{\lambda} + \mathcal{O}\left(\frac{1}{\lambda^2}\right). \tag{4.16}$$

The action values at these saddle points are

$$S(\sigma_{\pm}^{n}) = N_f\left[\pm i\lambda m + (2n+1)\pi\lambda - \log\lambda + 1 + \log(i\sinh m)\right] + \mathcal{O}\left(\frac{1}{\lambda}\right). \tag{4.17}$$

We are interested in the perturbative coefficients in the leading order of the large-λ limit. Let us expand the action around the saddle points:

$$S(\sigma) = S(\sigma_{\pm}^{n}) + \sum_{n=2}^{\infty}\frac{1}{n!}S^{(n)}(\sigma_{\pm}^{n})\delta\sigma^{n}, \tag{4.18}$$

where we regard $\delta\sigma = \mathcal{O}(N_f^{-1/2})$, and the first few derivatives of the action are

$$\begin{aligned}
S(\sigma) &= N_f\left[-i\lambda\sigma + \log(\cosh\sigma + \cosh m)\right],\\
S^{(1)}(\sigma) &= N_f\left[-i\lambda + \frac{\sinh\sigma}{(\cosh\sigma + \cosh m)}\right],\\
S^{(2)}(\sigma) &= N_f\left[\frac{\cosh\sigma}{(\cosh\sigma + \cosh m)} - \frac{\sinh^2\sigma}{(\cosh\sigma + \cosh m)^2}\right].
\end{aligned} \tag{4.19}$$

Noting that

$$\left.\frac{1}{\cosh\sigma + \cosh m}\right|_{\sigma=\sigma_{\pm}^{n}} \simeq \mp i\frac{\lambda}{\sinh m}, \tag{4.20}$$

we can approximate $S^{(n)}(\sigma_{\pm}^{n})$ as

$$S^{(n)}(\sigma_{\pm}^{n}) \simeq -N_f(-1)^n(n-1)!\left(\frac{\sinh\sigma}{\cosh\sigma + \cosh m}\right)^{n}\Bigg|_{\sigma=\sigma_{\pm}^{n}} = -N_f(n-1)!(i\lambda)^n. \tag{4.21}$$

Therefore, the action becomes

$$\begin{aligned}
S[\sigma] &\simeq S[\sigma_{\pm}^{n}] - N_f\sum_{n=2}^{\infty}\frac{1}{n}(i\lambda\delta\sigma)^n\\
&= S[\sigma_{\pm}^{n}] + N_f\left(i\lambda\delta\sigma + \log(1 - i\lambda\delta\sigma)\right).
\end{aligned} \tag{4.22}$$

Then, the perturbative series in the large-λ limit is generated by

$$F(N_f;\lambda) = \int_{-\infty}^{\infty} d\delta\sigma\; e^{-N_f(i\lambda\delta\sigma + \log(1 - i\lambda\delta\sigma))}. \tag{4.23}$$

One can rewrite this integral in the form of a Laplace transformation as in the Borel resummation formula if we make a change of variable as

$$t = i\lambda\delta\sigma + \log(1 - i\lambda\delta\sigma). \tag{4.24}$$

Noting that this equation is rewritten as

$$-e^{t-1} = (i\lambda\delta\sigma - 1)e^{i\lambda\delta\sigma - 1}, \tag{4.25}$$

we can write the solution as

$$\delta\sigma = \frac{1}{i\lambda}\left(1 + W(-e^{t-1})\right), \tag{4.26}$$

where $W(z)$ is the Lambert W function defined as a solution of

$$z = ue^u \quad \Leftrightarrow \quad u = W(z). \tag{4.27}$$

Then, using

$$\frac{dW(z)}{dz} = \frac{W(z)}{z(1+W(z))}, \tag{4.28}$$

we find

$$F(N_f;\lambda) = \frac{1}{i\lambda}\int dt\, e^{-N_f t}\frac{W(-e^{t-1})}{1+W(-e^{t-1})}. \tag{4.29}$$

It seems natural to identify

$$\widetilde{\mathcal{B}F}(t) = \frac{1}{i\lambda}\frac{W(-e^{t-1})}{1+W(-e^{t-1})}. \tag{4.30}$$

Some important features of the Lambert W function are:

- $W(z)$ has a branch cut along $(-\infty, -e^{-1})$.
- $W(-e^{-1}) = -1$.
- The small-z expansion of $W(z)$ has a radius of convergence e^{-1}.

Thus, the Borel transformation in the large-λ limit has the branch cut singularities at

$$t = 2\pi i\mathbb{Z}. \tag{4.31}$$

One might wonder why we now do not have the singularities beyond the imaginary axis which appeared in the numerical study represented in Fig. 5. This is because of the large-λ limit: the singularities beyond the imaginary axis go to infinity as $\lambda \to \infty$. This is most transparent in the formula in Eq. (4.17) for the asymptotic behaviors for the action.

We can see that the above Borel singularities come from the branch cuts in the σ-plane as follows. The variable t of the Borel plane is related to the σ-plane by the map in Eq. (4.26). Therefore, the origin $t = 0$ is associated with a saddle $\delta\sigma = 0$, while infinity is associated with the branch cut singularity $\delta\sigma = 1/i\lambda$. An interval $[0, 2\pi i]$ is associated with a closed loop which starts from the saddle $\delta\sigma = 0$ and runs around the branch cut singularity $\delta\sigma = 1/i\lambda$ back to the saddle. Since there is a logarithmic branch cut on the $\delta\sigma$-plane, we reach the next Riemann sheet once we move along the closed loop. Thus, the Borel singularities at $t = 2\pi i\mathbb{Z}$ are associated with the saddles on the different Riemann sheets. Such a relation should hold even when λ is not large, as long as we are in the supercritical region.

The above structures technically come from the fact that the action in Eq. (2.4) has a periodic structure and the logarithm branch cuts. Physically this type of factor originates from one-loop

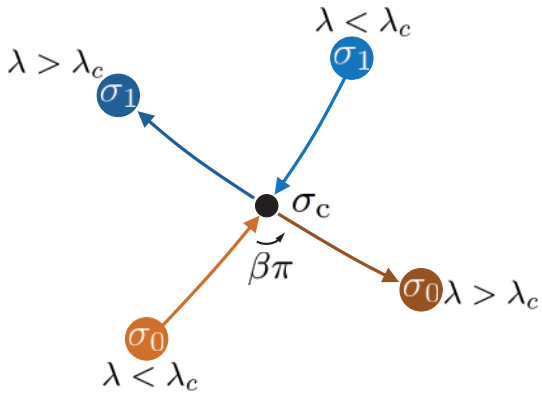

Fig. 6. An illustration of collision and scattering of saddles for $n = 2$. As the parameter λ is varied through the critical point $\lambda = \lambda_c$, two saddles σ_0, σ_1 collide at $\sigma = \sigma_c$ and are scattered with an angle $\beta\pi$.

contributions of hypermultiplets in the localization formula of S^3 partition functions [155–157]. This indicates that the above structures hold not only for SQED but also for more general supersymmetric gauge theories.

5. Lessons from 3d $\mathcal{N} = 4$ SQED

In this section, given the lessons from SQED obtained in the previous sections, we provide a more generic discussion on relations between resurgence and phase transitions. In particular, we discuss how the orders of phase transitions are described from the viewpoint of (anti-)Stokes phenomena.

5.1. Phase transitions as collisions of saddles

Let us consider a generic theory whose partition function is described by a one-dimensional integral of the form

$$e^{-NF(\lambda)} = \int d\sigma\, e^{-N\tilde{S}(\lambda;\sigma)}, \tag{5.1}$$

where $\tilde{S}(\lambda;\sigma)$ is the "action" and (N, λ) are some parameters specifying the theory. Suppose that the theory undergoes a phase transition at $\lambda = \lambda_c$ in the limit $N \to \infty$, accompanying a collision and a scattering of n saddles at $\sigma = \sigma_c$. We do not consider phase transitions simply by anti-Stokes phenomena, which have been often discussed in the context of Lefschetz thimble analysis. Here we show that the order of phase transition is determined by the scattering angle of the saddles. More specifically, we prove the following statement: if the n saddles collide and scatter with a scattering angle $\beta\pi$ as we vary the parameter λ through the critical point $\lambda = \lambda_c$ (as illustrated in Fig. 6), then we have the phase transition of order $\lceil (n+1)\beta \rceil$, where $\lceil x \rceil$ is the smallest integer greater than or equal to x.

Before moving on to the proof, let us recall some basics on phase transition. We have a pth-order phase transition at $\lambda = \lambda_c$ when the pth derivative of the "free energy" $F(\lambda)$ becomes singular at $\lambda = \lambda_c$ given its non-singular lower derivatives; that is,

$$\left|F^{(p)}(\lambda_c \pm 0)\right| = \infty \quad \text{or} \quad F^{(p)}(\lambda_c - 0) \neq F^{(p)}(\lambda_c + 0), \tag{5.2}$$

with

$$\left|F^{(k<p)}(\lambda_c \pm 0)\right| < \infty \quad \text{and} \quad F^{(k<p)}(\lambda_c - 0) = F^{(k<p)}(\lambda_c + 0). \tag{5.3}$$

The order p is related to the behavior of the free energy around the critical point as follows. Suppose that the free energy is expanded around the critical point as

$$F(\lambda = \lambda_{\rm c} + \delta\lambda) \simeq \begin{cases} C + A(\delta\lambda)^{\gamma} & \text{for } \delta\lambda < 0, \\ C + B(\delta\lambda)^{\gamma} & \text{for } \delta\lambda > 0, \end{cases} \tag{5.4}$$

where A, B, and C are complex constants and $\gamma > 0$. Note that the free energy is not necessarily real since it is not necessarily interpreted as the thermodynamic free energy for QFT on a generic manifold.[14] If $\gamma \notin \mathbb{Z}$, the phase transition is of order $p = \lceil \gamma \rceil$. Similarly, if $\gamma \in \mathbb{Z}$ and $A \neq B$, then the order of the phase transition is $p = \lceil \gamma \rceil$ while there is no phase transition for $A = B$. In what follows, we consider only the case with $A \neq B$ and the exponent γ independent of the sign of $\delta\lambda$. This is a consequence of a saddle collision, as we will see soon.

Now we provide the proof. As mentioned above, we are interested in the situation where the n saddles collide and scatter at $\sigma = \sigma_{\rm c}$ in varying the parameter λ through the critical point $\lambda_{\rm c}$. This means that the saddle point equation at $\lambda = \lambda_{\rm c}$ has a root with the degeneracy n. Therefore, the action around $\sigma = \sigma_{\rm c}$ is expanded as[15]

$$\tilde{S}(\lambda; \sigma = \sigma_{\rm c}) = a_0(\lambda) + a_1(\lambda)\delta\sigma + \cdots + a_{n+1}(\lambda)\delta\sigma^{n+1} + \cdots . \tag{5.5}$$

The coefficient $a_i(\lambda)$ is constrained by the condition that the saddles collide at $\lambda = \lambda_{\rm c}$ as

$$a_i(\lambda) = c_i \delta\lambda^{\alpha_i} + \cdots . \tag{5.6}$$

Without loss of generality, one can shift the action by an appropriate constant to make $a_0(\lambda)$ independent of λ:

$$a_0(\lambda) = c_0. \tag{5.7}$$

Furthermore, using the condition that the saddle point equation has a root with degeneracy n, we find

$$a_i(\lambda_{\rm c}) = 0 \qquad (i = 1, \ldots, n), \tag{5.8}$$

$$a_{n+1}(\lambda_{\rm c}) \neq 0. \tag{5.9}$$

Combining the above conditions for the coefficient leads us to

$$c_i = 0, \quad \text{or} \quad c_i \neq 0,\ \alpha_i > 0 \quad (i = 1, \ldots, n), \tag{5.10}$$

$$c_{n+1} \neq 0,\ \alpha_{n+1} = 0. \tag{5.11}$$

Solving the saddle point equation

$$0 = a_1(\lambda) + \cdots + (n+1)a_{n+1}(\lambda)\delta\sigma^n + \cdots \tag{5.12}$$

around the collision point $\delta\sigma = 0$, the saddle point around the critical point is simply written as

$$\delta\sigma_m \simeq s_m \delta\lambda^{\beta} \qquad (m = 0, \ldots, n-1), \tag{5.13}$$

[14] It is interpreted as the thermodynamic free energy when QFT is put on a manifold including S^1.
[15] Note that the configuration $\sigma = \sigma_{\rm c}$ is not a saddle point for $\lambda \neq \lambda_{\rm c}$ generically.

where s_m is a some constant and

$$\beta = \min\left(\frac{\alpha_1}{n}, \frac{\alpha_2}{n-1}, \ldots, \frac{\alpha_n}{1}\right). \tag{5.14}$$

Around the critical point $\delta\lambda = 0$, each saddle acquires a phase $(-1)^\beta$. This implies that the n saddles collide and scatter with an angle $\beta\pi$. Then, the action at the saddle σ_m takes the value

$$\tilde{S}_m \simeq c_0 + T_m(\delta\lambda)^{(n+1)\beta}, \tag{5.15}$$

with a constant T_m.

At the phase transition point there is a jump of the contributing saddle points in various ways. For example, in the case where the contributing saddles jump as $\sigma_0 \to \sigma_1$, the free energy changes as

$$F \simeq \begin{cases} c_0 + T_0(\delta\lambda)^{(n+1)\beta} & \text{for } \delta\lambda < 0, \\ c_0 + T_1(\delta\lambda)^{(n+1)\beta} & \text{for } \delta\lambda > 0. \end{cases} \tag{5.16}$$

In the case where the contributing saddles jump as $\sigma_0 \to \sigma_0, \ldots, \sigma_{n-1}$, the free energy changes as

$$F \simeq \begin{cases} c_0 + T_0(\delta\lambda)^{(n+1)\beta} & \text{for } \delta\lambda < 0, \\ c_0 + (T_0 + \cdots + T_{n-1})(\delta\lambda)^{(n+1)\beta} & \text{for } \delta\lambda > 0. \end{cases} \tag{5.17}$$

In any case, the phase transition is of order $\lceil (n+1)\beta \rceil$, and this completes the proof. Our argument also shows a connection between the order of the phase transition and the anti-Stokes line. The formula in Eq. (5.15) for the action shows that the anti-Stokes line is given by $\Re\left[(\delta\lambda)^{(n+1)\beta}\right] = 0$. Thus, one can also read off the order of the phase transition by looking at the anti-Stokes line.

5.2. *Thimbles and Borel singularities around critical points*

In this subsection we demonstrate the discussion in the last subsection using the integral representation of the Airy function whose "action" is given by

$$\tilde{S}(\lambda;\sigma) = \frac{i\sigma^3}{3} - i\lambda\sigma. \tag{5.18}$$

We refer to this example as the Airy-type model. As we will see soon, this example corresponds to $n = 2$, $\alpha = 1/2$, and has common features with the SQED Eq. (2.1) in the context of the argument in this section.

5.2.1. *Lefschetz thimbles*

The Airy-type model corresponds to

$$c_0 = 0, \qquad c_1 = -i, \qquad \alpha_1 = 1, \qquad c_2 = 0, \qquad c_3 = \frac{i}{3}, \qquad \alpha_3 = 0. \tag{5.19}$$

The saddle points in this example are simply given by

$$\sigma_\pm = \pm\lambda^{1/2}, \tag{5.20}$$

which indicates that the two saddles collide at $\sigma = 0$ for $\lambda = 0$. Therefore, in the notation of the previous subsection, we have

$$\sigma_c = 0, \qquad \lambda_c = 0, \qquad \delta\sigma_\pm = \pm\delta\lambda^{1/2}, \tag{5.21}$$

and

$$n = 2, \qquad \alpha = \frac{1}{2}. \tag{5.22}$$

The action at the saddle $\sigma_\pm$ is given by

$$\tilde{S}_\pm = \mp \frac{2i}{3} (\delta\lambda)^{3/2}. \tag{5.23}$$

This leads us to the standard Airy-type Stokes graph

$$\text{Stokes line: } \Im[i(\delta\lambda)^{3/2}] = 0, \qquad \text{Anti-Stokes line: } \Re[i(\delta\lambda)^{3/2}] = 0. \tag{5.24}$$

We can find the (dual) thimbles by solving

$$\mathcal{J}_\pm : \frac{d\sigma}{ds} = \overline{\frac{dS(\sigma)}{d\sigma}}\bigg|_{\sigma \simeq \sigma_\pm}, \qquad \mathcal{K}_\pm : \frac{d\sigma}{ds} = -\overline{\frac{dS(\sigma)}{d\sigma}}\bigg|_{\sigma \simeq \sigma_\pm}. \tag{5.25}$$

In Fig. 7 we show how the thimbles change as the phase $\arg(\delta\lambda)$ increases. As $\arg(\delta\lambda)$ is increased from a negative value we encounter a Stokes phenomenon at $\arg(\delta\lambda) = -\pi$, an anti-Stokes phenomenon at $\arg(\delta\lambda) = -2\pi/3$, a Stokes phenomenon at $\arg(\delta\lambda) = -\pi/3$, and an anti-Stokes phenomenon at $\arg(\delta\lambda) = 0$. In particular, we observe a jump of the contributing saddles at $\arg(\delta\lambda) = -\pi/3$ (as well as $\arg(\delta\lambda) = +\pi/3$): we have a contribution only from $\sigma = \sigma_+$ for $\arg(\delta\lambda) < -\pi/3$ while we have contributions from the two saddles $\sigma = \sigma_+$ and $\sigma = \sigma_-$ at $\arg(\delta\lambda) = -\pi/3 + 0$. This is a manifestation of the Stokes phenomenon. The free energy also jumps as

$$F \simeq \begin{cases} \tilde{S}_+ & = \frac{2}{3}(-\delta\lambda)^{3/2} \quad \text{for } \delta\lambda < 0, \\ \tilde{S}_+ + \tilde{S}_- & = 0 \qquad\qquad\quad \text{for } \delta\lambda > 0, \end{cases} \tag{5.26}$$

which implies a second-order phase transition.

Next, let us increase $\delta\lambda$ from -1 to 1, keeping $\Im\delta\lambda = 0$. As $\delta\lambda$ goes from -1 to 0, the two saddles (in the top left panel of Fig. 7) approach the origin along the imaginary axis. At $\delta\lambda = 0$, they collide and change their directions. As $\delta\lambda$ goes from 0 to $+1$, the two saddles (in the bottom right panel of Fig. 7) depart the origin along the real axis. In other words, the two saddles collide with an angle $\pi/2$ at the phase transition. Also, we remark that, during the phase transition, we cross the anti-Stokes line $\arg(\delta\lambda) = -2\pi/3$ and the Stokes line $\arg(\delta\lambda) = -\pi/3$. Thus, the second-order phase transition is understood as a phenomenon in which an anti-Stokes and a Stokes phenomenon occur simultaneously. To summarize, the second-order phase transition in the Airy-type model is interpreted as follows:

(1) Contributing saddles jump as $\sigma_+ \to \sigma_+, \sigma_-$.
(2) The two saddles collide and scatter with a scattering angle $\pi/2$.
(3) A Stokes phenomenon and an anti-Stokes phenomenon occur simultaneously.

5.2.2. Borel singularities

The "partition function" of the Airy-type model is defined as

$$Z(\lambda) = \int d\sigma \, e^{-N\tilde{S}(\lambda;\sigma)}. \tag{5.27}$$

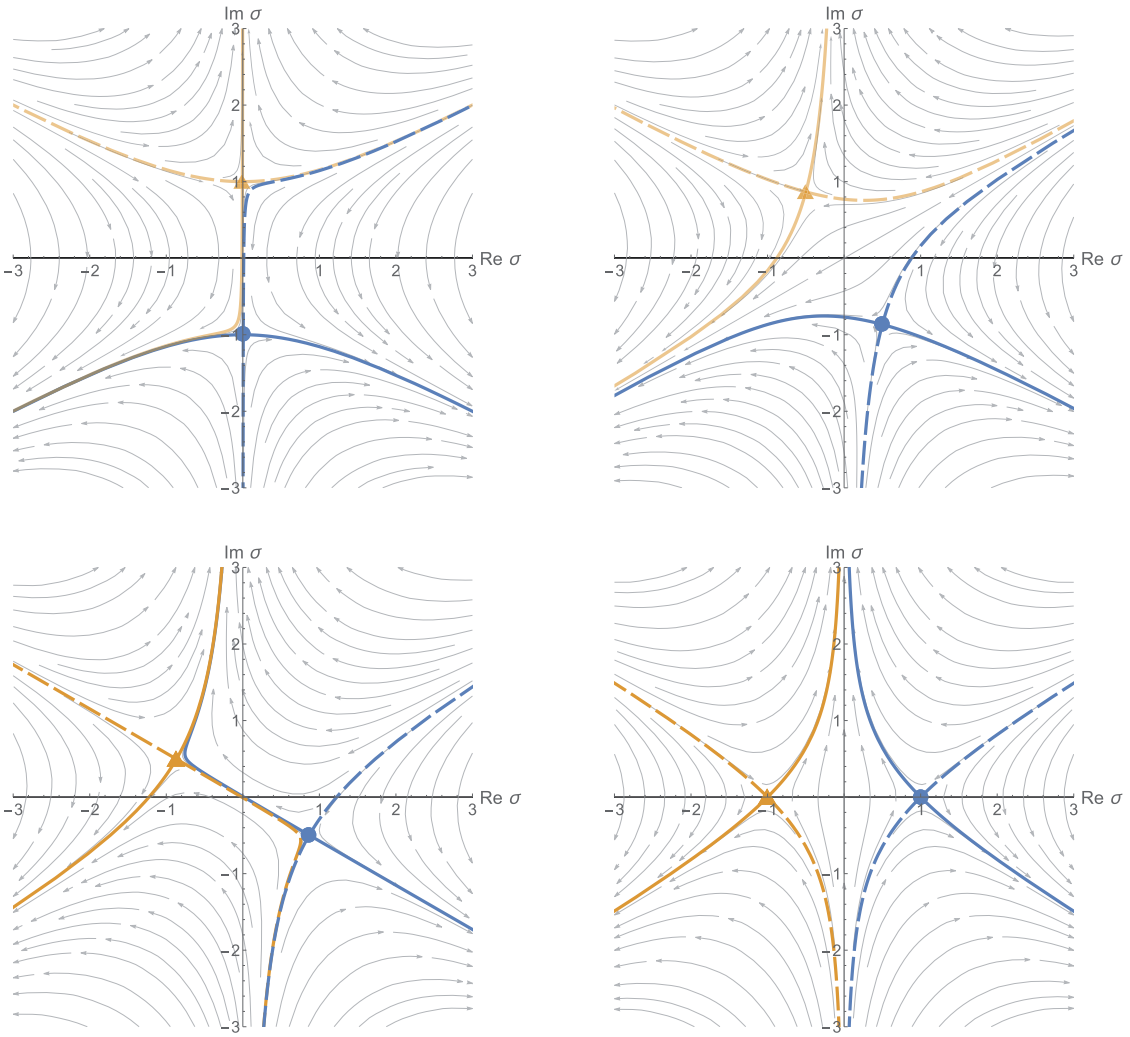

Fig. 7. Illustrations of the thimble structures of the Airy-type model for $|\delta\lambda| = 1$. The blue circle and orange triangle symbols indicate the saddles σ_0 and σ_1, respectively. The Lefschetz thimbles associated with them are drawn as lines with the same colors. The dual thimbles are drawn as dashed lines. The opaque saddles and thimbles contribute to the integral, while the translucent ones do not. The phase of $\delta\lambda$ is $\arg(\delta\lambda) = -\pi + 0.01$ (top left), $-2\pi/3$ (top right), $-\pi/3 + 0.01$ (bottom left), and 0 (bottom right).

Let us consider the $1/N$ expansion around the "trivial" saddle $\sigma_+ = \lambda^{1/2}$. Using the formula in App. A, the perturbative series is formally given by

$$\int_{\mathcal{J}_+} d\sigma\, e^{-N\tilde{S}(\lambda;\sigma)} = \sqrt{\frac{\pi}{i\lambda^{1/2}N}} e^{\frac{2i\lambda^{3/2}}{3}N} F\left(\frac{1}{N}\right), \tag{5.28}$$

where

$$F\left(\frac{1}{N}\right) = \sum_{l=0}^{\infty} \frac{a_l}{N^l}, \qquad a_l = \frac{\Gamma(3l+1/2)}{3^{2l}(-i\lambda^{3/2})^l \Gamma(1/2)\Gamma(2l+1)}. \tag{5.29}$$

Note that the coefficient grows factorially. The analytic continuation of its Borel transformation is

$$\widetilde{\mathcal{B}F}(t) = {}_2F_1\left(\frac{1}{6}, \frac{5}{6}, 1; \frac{3t}{4(-i\lambda^{3/2})}\right). \tag{5.30}$$

This function has a Borel singularity (branch cut singularity) at

$$t = \frac{4(-i\lambda^{3/2})}{3}. \tag{5.31}$$

This Borel singularity corresponds to the "non-trivial saddle" $\sigma_- = -\lambda^{1/2}$, and it collides with the origin corresponding to the "trivial saddle" at the critical point $\lambda = 0$. The scattering angle is $-3\pi/2 \sim \pi/2$. After the collision ($\lambda > 0$), the Borel singularity is on the imaginary axis. This means that an anti-Stokes phenomenon occurs: $\Re\tilde{S}_+ = \Re\tilde{S}_- = 0$. Thus, the collision of saddles is appropriately encoded in the perturbative series as expected by the resurgence theory.

5.3. Second-order SQED phase transition revisited

In this section we revisit the second-order phase transition in SQED based on the previous subsections to further clarify the relationship between phase transition and resurgence.

5.3.1. Lefschetz thimble analysis

From the Lefschetz thimble analysis in Sect. 3, we have seen that the SQED around the second-order phase transition point has the following properties:

(i) Contributing saddle points jump as $\sigma_0^+ \to \sigma_0^+, \sigma_0^-$.
(ii) The two saddles collide and scatter with scattering angle $\pi/2$.
(iii) An infinite number of Stokes phenomena associated with saddles $\sigma_{n>0}^{\pm}$ occur.

The first two points are common with the Airy-type model in the previous subsection. This is because the SQED "action" in Eq. (2.4) has a similar expansion to one of the Airy-type models around the critical point. Thus, the second-order SQED phase transition is interpreted in a similar way as the Airy-type model. The third point is particular for SQED. The difference essentially comes from the fact that SQED has an infinite number of saddles periodically distributed along the imaginary axis. Once thimbles run along the imaginary axis after a phase transition, they inevitably pass through the periodic saddles. Such thimble behavior causes an infinite number of Stokes phenomena. Technically the appearance of the periodic saddles is due to the cosh factors originating from the one-loop determinant of the hypermultiplets in the SUSY localization of the S^3 partition function. Therefore, we expect that the above features also appear in other SUSY gauge theories on S^3.

5.3.2. Borel resummation

In the language of the Borel resummation, the second-order phase transition has the following features:

(I) In the supercritical region, the two Borel singularities line up along the imaginary axis on the Borel plane.
(II) The two Borel singularities collide and scatter with a scattering angle $\pi/2$ as we cross the critical point.
(III) The $1/N_f$ expansion becomes Borel non-summable along the positive real axis in the supercritical region.

(I), (II), and (III) here correspond to (i), (ii), and (iii) of the Lefschetz thimble analysis, respectively, as expected from the resurgence theory. The first point means that the saddle points associated

with the Borel singularities along the imaginary axis have the same real part of the actions and therefore contribute to the integral with equal weights in the supercritical region. The second point is a counterpart of the collision of two saddles from the viewpoint of the Borel resummation. The relation between Borel singularities and saddle points implies that the collision of two saddles in the σ-plane leads to one of the two Borel singularities in the t-plane. Thus, we can also decode the order of the phase transition purely from how the Borel singularities collide. The third point means that the thimbles cross the multiple saddle points for $\arg(N_f) = 0$ as shown in Fig. 1. In the SQED case, the Borel non-summability detects the infinite number of periodic saddles which come from the contribution from the hypermultiplets.

Finally, let us consider the Stokes graph. The second-order phase transition is interpreted in terms of the Stokes graph as follows:

- The anti-Stokes line is given by $\Re[(\delta\lambda)^{3/2}] = 0$.
- A Stokes phenomenon and an anti-Stokes phenomenon associated with saddles $\sigma_0^{\pm}$ occur simultaneously.

These points are analogous to the Airy-type model discussed in Sect. 5.2. The only difference is that the infinite number of Stokes phenomena associated with $\sigma_{n>0}^{\pm}$ occur simultaneously.

6. Conclusions and discussion

We have studied the resurgence structure of a quantum field theory with a phase transition to uncover relations between resurgence and phase transitions. In particular, we focused on three-dimensional $\mathcal{N} = 4$ SQED, which undergoes the second-order quantum phase transition in the large-flavor limit [143]. We approached the problem from the viewpoints of the Lefschetz thimbles and Borel resummation. In the Lefschetz thimble approach, we specifically studied the thimble structures of the integral representation of the partition function obtained by the supersymmetric localization [155–157]. We first justified the assumption in Ref. [143] that all the dominant complex saddles contribute to the integral by the Lefschetz thimble analysis. Then we found that there is a collision of the two saddles and a jump of the contributing saddle points as we cross the critical value of the parameter $\lambda = \eta/N_f$. While this is the Stokes phenomenon, we saw that an anti-Stokes phenomenon also occurs at the same time. Thus, we interpret the second-order phase transition as simultaneous Stokes and anti-Stokes phenomena. Our result also shows that the phase transition accompanies an infinite number of Stokes phenomena associated with the other saddles. This behavior technically comes from the fact that the action in Eq. (2.4) has a periodic structure which originates physically from one-loop contributions of hypermultiplets in the localization formula of S^3 partition functions. This indicates that the above structures hold not only for SQED but also for more general supersymmetric gauge theories.

In the Borel resummation approach, we saw that the thimble structures are appropriately mapped to the Borel plane structures of the large-flavor expansion, as expected from the resurgence theory. We found the Borel singularities, two of which correspond to the two saddles. The two Borel singularities line up vertically along the imaginary axis after the phase transition. This is a sign that the two saddles contribute to the integral with equal weights. At the phase transition, the two Borel singularities collide as the two saddles. The scattering angle of the Borel singularities at the collision is related to the order of the phase transition. We also saw that the large-flavor expansion becomes Borel non-summable along the positive real axis in the supercritical region, due to an infinite number of Borel singularities. This reflects the infinite number of Stokes phenomena.

Given the lessons from SQED, we provided more generic discussion on the relations between resurgence and phase transitions. We considered a one-dimensional integral of the form in Eq. (5.1) and showed that if the n saddles collide and scatter with a scattering angle $\beta\pi$ as we vary the parameter λ through the critical point $\lambda = \lambda_c$, then we have a phase transition of order $\lceil (n+1)\beta \rceil$. Our argument also showed that we have anti-Stokes phenomena at the critical point, where the anti-Stokes line is given by $\Re\left[(\delta\lambda)^{(n+1)\beta}\right] = 0$. This implies that one can also read off the order of the phase transition by looking at the anti-Stokes line. We also argued that the above behaviors are naturally translated into the language of the Borel plane. This means that the order of phase transitions can also be determined by tracking how Borel singularities move as the parameter varies. This implies that we can read off information on phase structures purely in terms of perturbative expansions. The above results apply to more general theories as long as they reduce to the form in Eq. (5.1).

Finally, we revisited the second-order SQED quantum phase transition from the above viewpoints. In the case of SQED, the two saddles σ_0^+ and σ_0^- collide and scatter with $\pi/2$ as we cross the critical point $\lambda = \lambda_c$. Therefore, we have $(n, \beta) = (2, 1/2)$ in the formula $\lceil (n+1)\beta \rceil$ for the order of the phase transition, and this agrees with the fact that the second-order phase transition occurs. From the viewpoint of Stokes graphs, the second-order phase transition is essentially described as the standard Airy-type graph. This clarifies that the second-order phase transition is understood as a phenomenon where Stokes and anti-Stokes phenomena occur at the same time. This is in clear contrast to the common understanding that a first-order phase transition is associated with an anti-Stokes phenomenon. All of the above results support that resurgence works for describing the second-order SQED phase transition.

We have obtained good news which may be useful in developing studies of resurgence on the technical side. Originally, the correspondence between saddles and Borel singularities in one-dimensional integrals was shown in Refs. [158–160]. It is not guaranteed that we can naively apply the correspondence to SQED because some of their assumptions are violated due to the logarithmic branch cuts in the action. Nevertheless, our results suggest that the correspondence still holds even in SQED. This seems to imply that one can extend the correspondence beyond the class of integrals studied in Refs. [158–160]. It would be interesting to pursue this direction.

We believe that our results give a good step forward in understanding the connections between phase transitions and resurgence. Yet there are still various questions and tasks which should be addressed as next steps. First, it is important to understand the physical meaning of the second-order SQED phase transition. For instance, we have not understood yet whether there is a change of symmetries around the critical point, whether the critical point describes some conformal field theory, and so on. Second, we have not identified interpretations of the saddle points in SQED in the language of the original path integral. It seems that they are closely related to the complex supersymmetric solutions found in Ref. [115], as discussed in App. F. We need further studies to clarify the relations more precisely. Third, it would be interesting to study the relations between Lee–Yang zeros and the Stokes graph. While the authors of Ref. [147] found that Lee–Yang zeros are on anti-Stokes curves in the zero-dimensional Gross–Neveu-like model, the SQED studied in this paper does not seem to have such a property. This may suggest that the situation in SQED is different from the zero-dimensional Gross–Neveu-like model. Fourth, it would be illuminating to study resurgence structures with respect to other SQED parameters such as the FI parameter η. There may be interesting relations to the resurgence structure of the large-flavor expansion as in the two-dimensional pure $U(N)$ Yang–Mills theory on the lattice, where interesting connections were found among expansions by $1/N$, Yang–Mills coupling, and 't Hooft coupling [81,148,149]. Finally,

it is technically important to improve the Padé-Uniformized approximation for cases with multiple branch cuts in Borel planes. It seems that improvement of the approximation is hindered by the non-trivial topology of Riemann sheets due to the branch cuts. Such a problem often arises in the context of resurgence and therefore further studies are desired.

While this paper has focused on connections between resurgence and phase transitions, more generally, it would be very interesting to explore relations between resurgence and phases themselves rather than their transitions. It is known that information on phases in quantum field theories are partially captured by 't Hooft anomalies, including phases beyond the Ginzburg–Landau or Nambu paradigm. While 't Hooft anomalies are typically easy to calculate and give quite robust information on phases, they rely on the existence of symmetries.[16] In contrast, analysis of resurgence does not require symmetries and gives detailed information while it is technically much more complicated. Therefore, they play complementary roles. In this paper we have discussed that some features of phase transitions are captured by qualitative behaviors of the objects appearing in the analysis of resurgence. It would be great if one can find similar connections for 't Hooft anomalies.[17] It might open a door to a shining world of non-perturbative physics.

Acknowledgments

The authors would like to thank Okuto Morikawa, Naohisa Sueishi, Hiromasa Takaura, and Yuya Tanizaki for valuable discussions. Preliminary results of this work have been presented in the KEK workshop "Thermal Quantum Field Theory and its Application" (August 2020), the YITP workshop YITP-W-20-08 "Progress in Particle Physics 2020" (September 2020), JPS meetings (September 2020 and March 2021), the YITP-RIKEN iTHEMS workshop YITP-T-20-03 "Potential Toolkit to Attack Nonperturbative Aspects of QFT: Resurgence and related topics" (September 2020), the 15th Kavli Asian Winter School on Strings, Particles and Cosmology (January 2021), and the Osaka City University Workshop "Randomness, Integrability and Representation Theory in Quantum Field Theory 2021" (March 2021). Discussions during the workshops were helpful in completing this work. M. H. is partially supported by MEXT Q-LEAP. This work is supported in part by Grant-in-Aid for Scientific Research (KAKENHI) (B) Grant Number 18H01217 (T. F., T. M., and N. S.). S. K. is supported by the Polish National Science Centre grant 2018/29/B/ST2/02457.

Funding

Open Access funding: SCOAP[3].

Appendix A. Details of the large-flavor expansion

In this appendix we compute the coefficients of the $1/N_f$ expansion of the partition function around a general saddle point σ_*. First, to make the N_f dependence transparent, we introduce

$$S(\sigma) = N_f \tilde{S}(\sigma). \tag{A.1}$$

[16] This is not necessarily true for "anomalies in the space of coupling constants," which was recently proposed [168,169].

[17] See Ref. [36] for a very recent work on quantum mechanics in a similar spirit.

Then we expand $\tilde{S}(\sigma)$ as

$$\tilde{S}(\sigma) = \tilde{S}(\sigma_*) + \frac{\tilde{S}''(\sigma_*)}{2!}(\sigma-\sigma_*)^2 + \sum_{k=0}^{\infty} \frac{\tilde{S}^{(k+3)}(\sigma_*)}{(k+3)!}(\sigma-\sigma_*)^{k+3}, \tag{A.2}$$

and regard the last term as a perturbation. Next, we rewrite the contribution from the saddle σ_* to the integral in Eq. (2.1) as

$$\begin{aligned}\int_{\mathcal{J}_*} d\sigma\, e^{-S(\sigma)} &= e^{-N_f\tilde{S}(\sigma_*)}\int_{\mathcal{J}_*} d\sigma \sum_{n=0}^{\infty}\frac{1}{n!}\left(-\sum_{k=0}^{\infty}\frac{N_f\tilde{S}^{(k+3)}(\sigma_*)}{(k+3)!}(\sigma-\sigma_*)^{k+3}\right)^n e^{-\frac{N_f\tilde{S}''(\sigma_*)}{2!}(\sigma-\sigma_*)^2} \\ &= e^{-N_f\tilde{S}(\sigma_*)}\sqrt{\frac{2}{N_f\tilde{S}''(\sigma_*)}}\int_{-\infty}^{\infty} d\xi \sum_{n=0}^{\infty}\frac{(-1)^n}{n!}\left(\sum_{k=0}^{\infty} c_k \frac{\xi^{k+3}}{N_f^{\frac{k+1}{2}}}\right)^n e^{-\xi^2},\end{aligned} \tag{A.3}$$

where $\mathcal{J}_*$ is the Lefschetz thimble associated with σ_* and

$$c_k = \frac{2^{\frac{k+3}{2}}}{(k+3)!}\frac{\tilde{S}^{(k+3)}(\sigma_*)}{\left(\tilde{S}''(\sigma_*)\right)^{\frac{k+3}{2}}}. \tag{A.4}$$

To proceed, we also introduce

$$\left(\sum_{k'=0}^{\infty} c_{k'}\epsilon^{k'}\right)^n \equiv \sum_{k=0}^{\infty}\tilde{c}_k(n)\epsilon^k. \tag{A.5}$$

Then, exchanging the integration and summation, the formal $1/N_f$ expansion is computed as

$$\begin{aligned} & e^{-N_f\tilde{S}(\sigma_*)}\sqrt{\frac{2}{N_f S''(\sigma_*)}}\sum_{n,k=0}^{\infty}\frac{(-1)^n\tilde{c}_k(n)}{n!}\frac{1}{N_f^{\frac{n+k}{2}}}\int_{-\infty}^{\infty} d\xi\, \xi^{3n+k}e^{-\xi^2} \\ &= e^{-N_f\tilde{S}(\sigma_*)}\sqrt{\frac{2\pi}{N_f\tilde{S}''(\sigma_*)}}\sum_{n,k=0,\ 3n+k=\text{even}}^{\infty}\frac{(-1)^n\Gamma\left(\frac{1}{2}+\frac{3n+k}{2}\right)\tilde{c}_k(n)}{\Gamma(1/2)\Gamma(n+1)}\frac{1}{N_f^{\frac{n+k}{2}}} \\ &= e^{-N_f\tilde{S}(\sigma_*)}\sqrt{\frac{2\pi}{N_f\tilde{S}''(\sigma_*)}}\sum_{\ell=0}^{\infty}\frac{a_\ell}{N_f^\ell}, \end{aligned} \tag{A.6}$$

where

$$a_\ell = \sum_{n=0}^{2\ell}\frac{(-1)^n\Gamma\left(\frac{1}{2}+\ell+n\right)\tilde{c}_{2\ell-n}(n)}{\Gamma(1/2)\Gamma(n+1)}. \tag{A.7}$$

Appendix B. Lefschetz thimble structures for larger arg(N_f)

In this appendix we study the thimble structures for larger values of $\theta = \arg(N_f)$ than in Sect. 3.2 to understand the Stokes phenomena more precisely. It appears that the larger $\arg(N_f)$ region is not directly related to the phase transition itself since originally the parameters were real. However, this is essential to understanding the Borel plane structures, as discussed in Sect. 4.

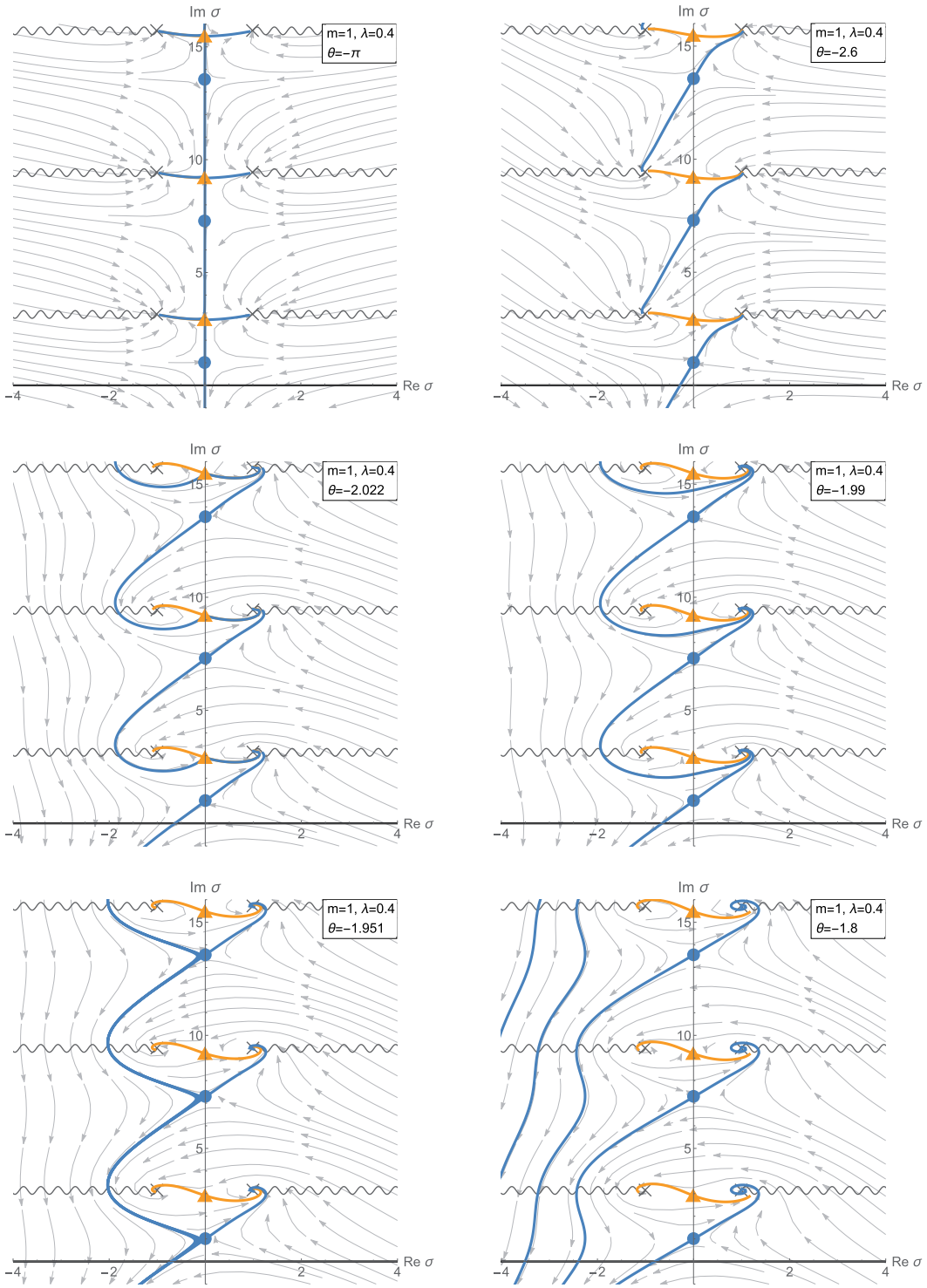

Fig. B.1. Illustrations of the Lefschetz thimble structures for the subcritical region $\lambda < \lambda_c$. (In these figures, $m = 1$, for which $\lambda = 0.4$.) Larger phases are given, $-\pi \leq \theta \leq 0$, so that we can observe Stokes phenomena (left) and thimble structures (right) between them. Reflecting the figures along the imaginary axis corresponds to flipping the sign of θ.

As mentioned at the end of Sect. 3.3, for non-small $\arg(N_f)$ we have to take the effects of the branch cuts into account. Namely, when thimbles cross the branch cuts, the action is shifted by $2\pi i N_f \mathbb{Z}$,

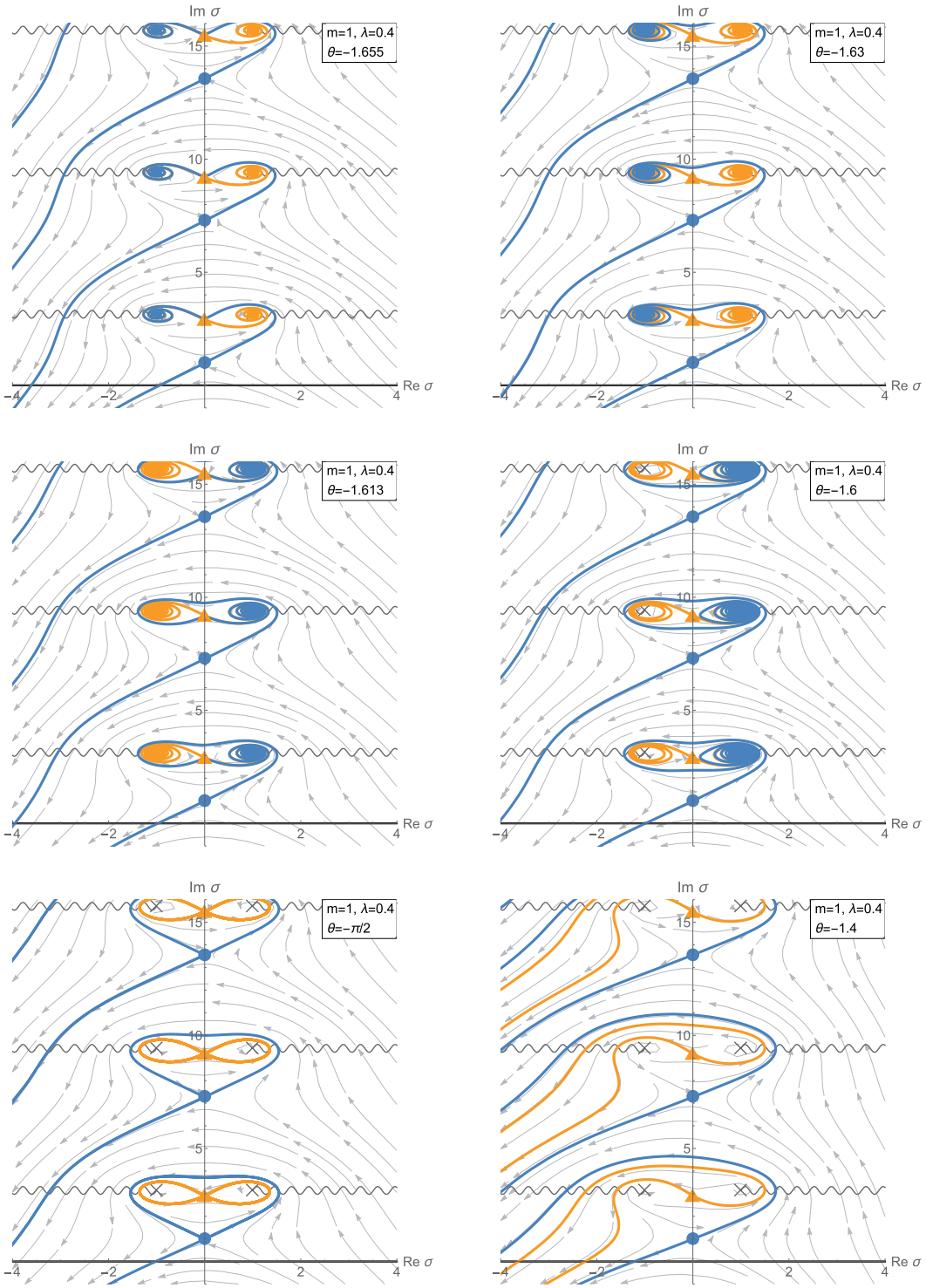

Fig. B.1. Continued.

and this effect modifies the condition for having Stokes phenomena. We will see soon that Stokes phenomena due to this effect indeed occur in this problem.

In Fig. B.1 we summarize the Lefschetz thimble structures for $(\lambda, m) = (0.4, 1)$ with various $-\pi < \arg(N_f) < 0$ as representative of the subcritical region $\lambda < \lambda_c$. Reflecting these figures along the vertical axis corresponds to flipping the sign of $\arg(N_f)$. Thus, these figures practically cover

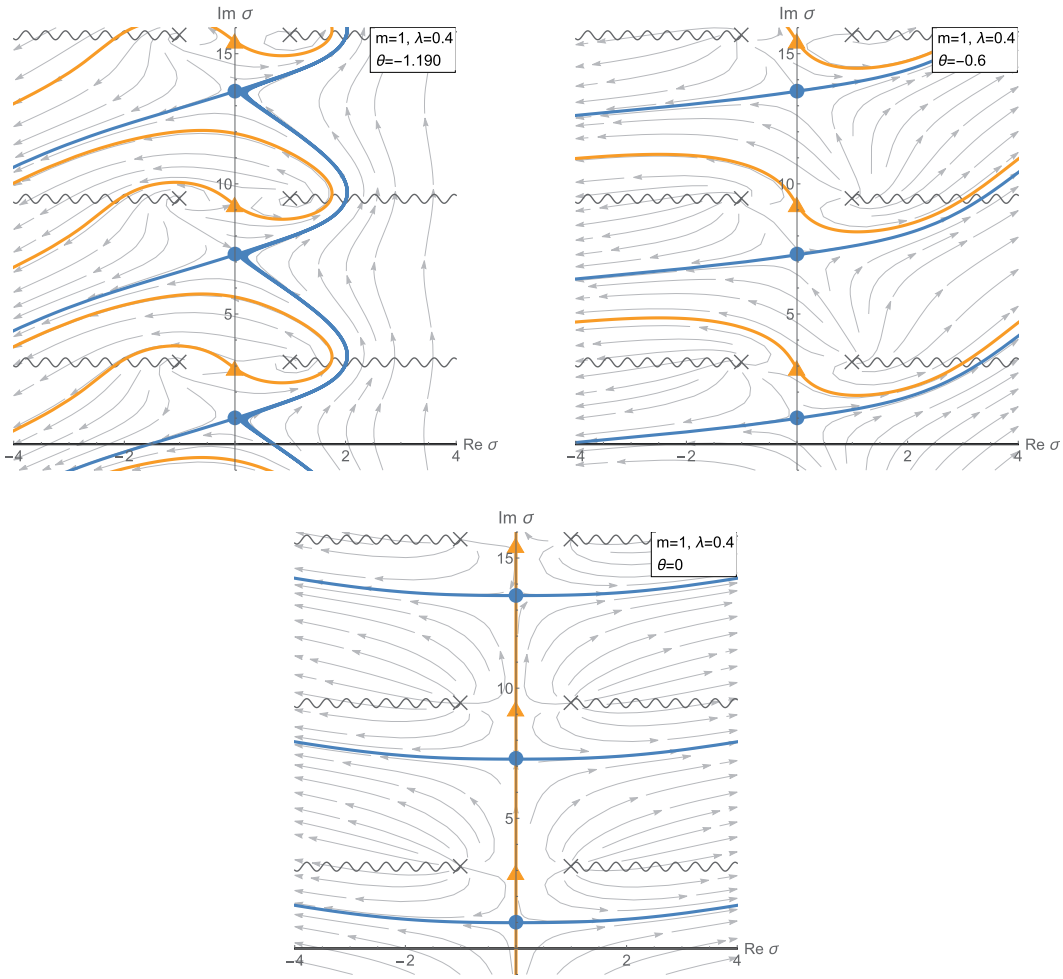

Fig. B.1. Continued.

the full region $-\pi \leq \arg(N_f) < +\pi$. In the figures on the left side, Stokes phenomena occur. For example, at $\arg(N_f) = -1.190$, the Lefschetz thimble associated with saddle σ_0^+ (blue line) passes also through other saddles $\sigma_{n>0}^+$. This is nothing but a Stokes phenomenon. One can easily check that the condition for having Stokes phenomena,

$$\Im[S(\sigma_{n>0}^+) - S(\sigma_0^+) + 2\pi i N_f \mathbb{Z}] = 0, \tag{B.1}$$

is satisfied by $\arg(N_f) = -1.190$.

In Fig. B.2 we summarize the thimble structures for the supercritical region $\lambda > \lambda_c$ with various $-\pi < \arg(N_f) < +\pi$ (specifically, $(\lambda, m) = (1.2, 1)$ in the figures). In the figures on the left side, Stokes phenomena occur. For example, at $\arg(N_f) = -0.039$ the Lefschetz thimble associated with the saddle σ_0^+ (blue line) passes also through another saddle σ_1^-. This means that

$$\Im[S(\sigma_1^-) - S(\sigma_0^+) + 2\pi i N_f \mathbb{Z}] = 0 \tag{B.2}$$

holds at $\arg(N_f) = -0.039$. This is also a Stokes phenomenon. These structures are consistent with the Borel plane structures discussed in Sect. 4.

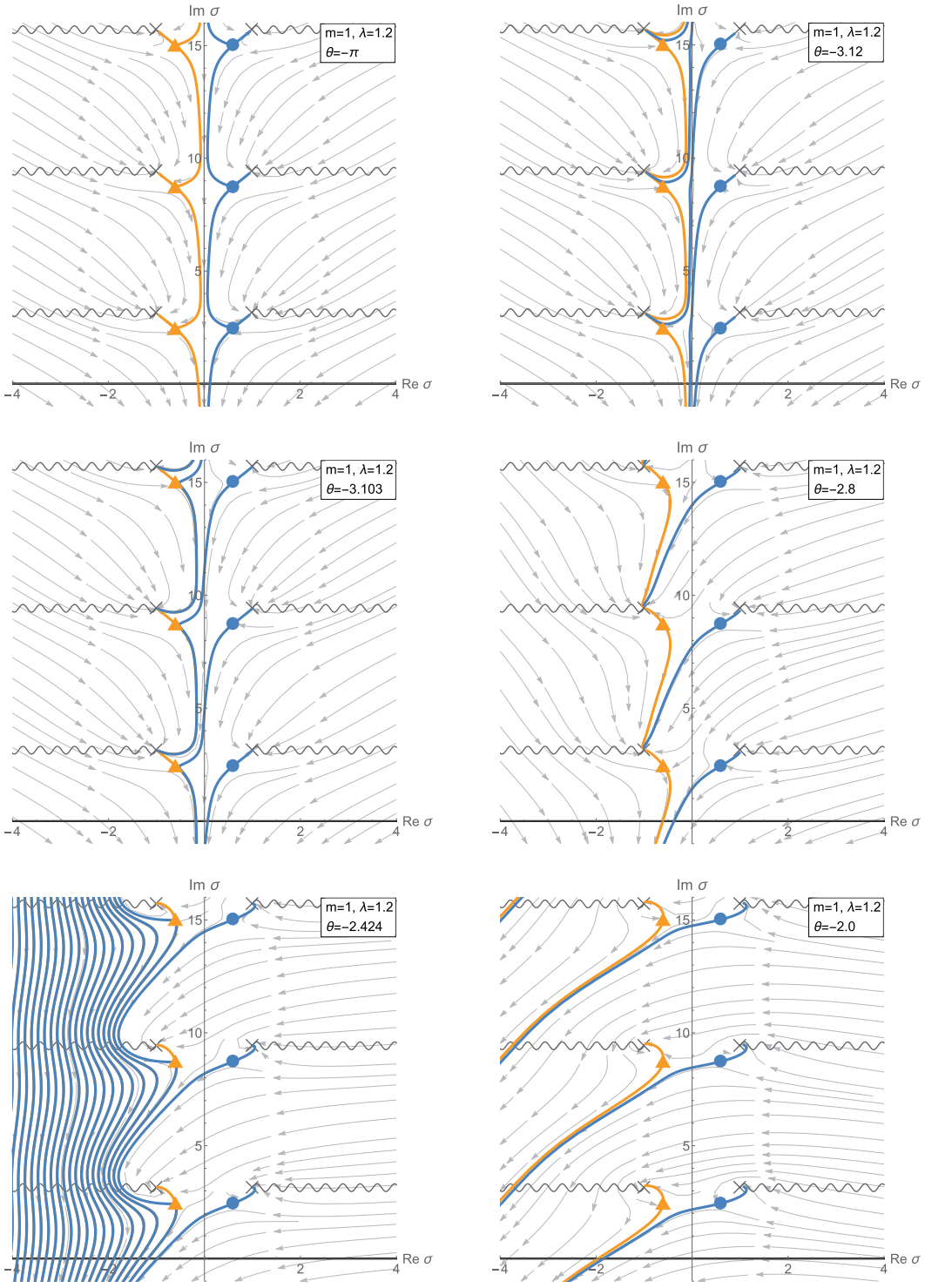

Fig. B.2. Illustrations of the Lefschetz thimble structures for the supercritical region $\lambda > \lambda_c$. (In these figures, $m = 1$, for which $\lambda = 0.4$.) Larger phases are given, $-\pi \leq \theta \leq 0$, so that we can observe Stokes phenomena (left) and thimble structures (right) between them.

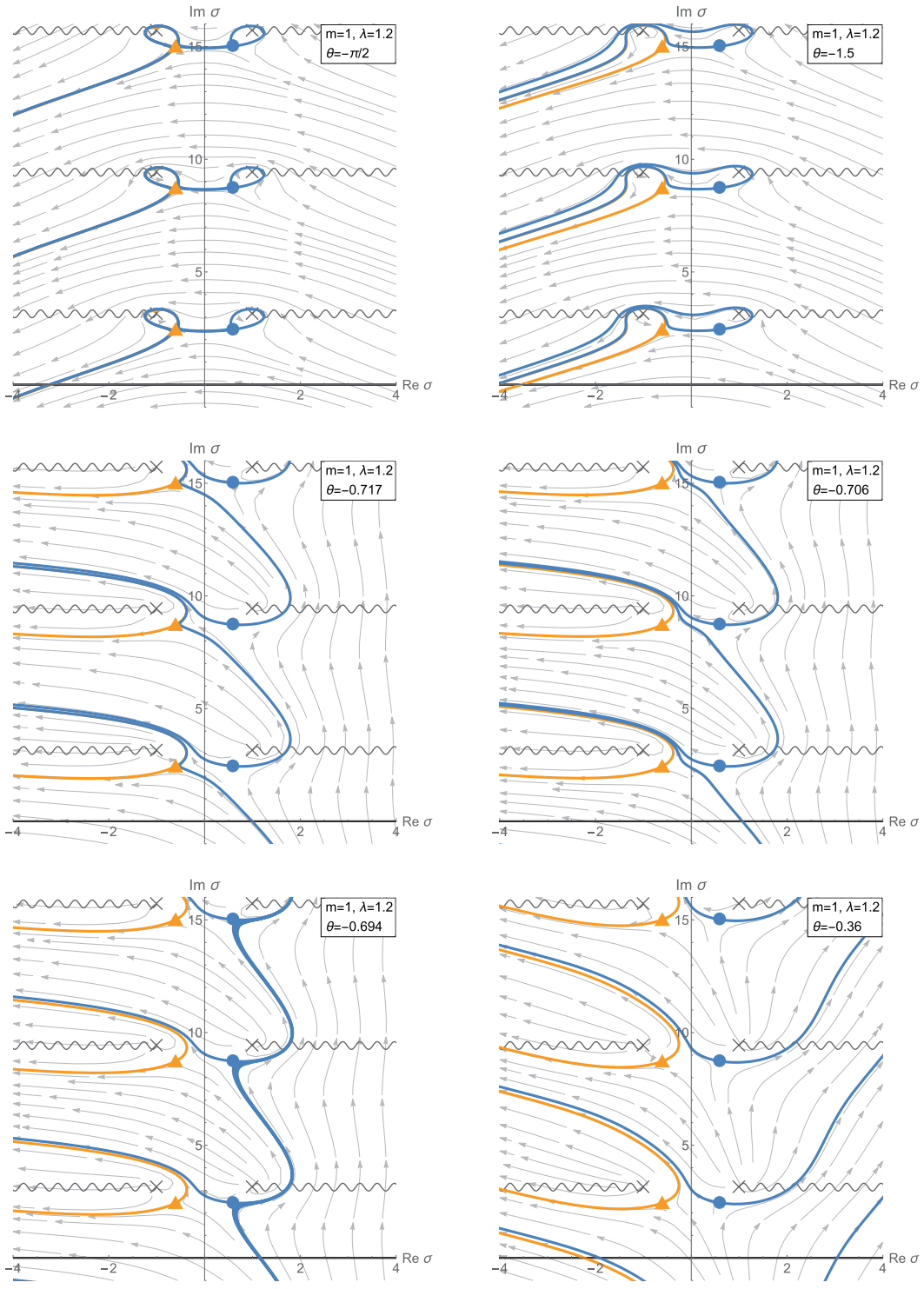

Fig. B.2. Continued.

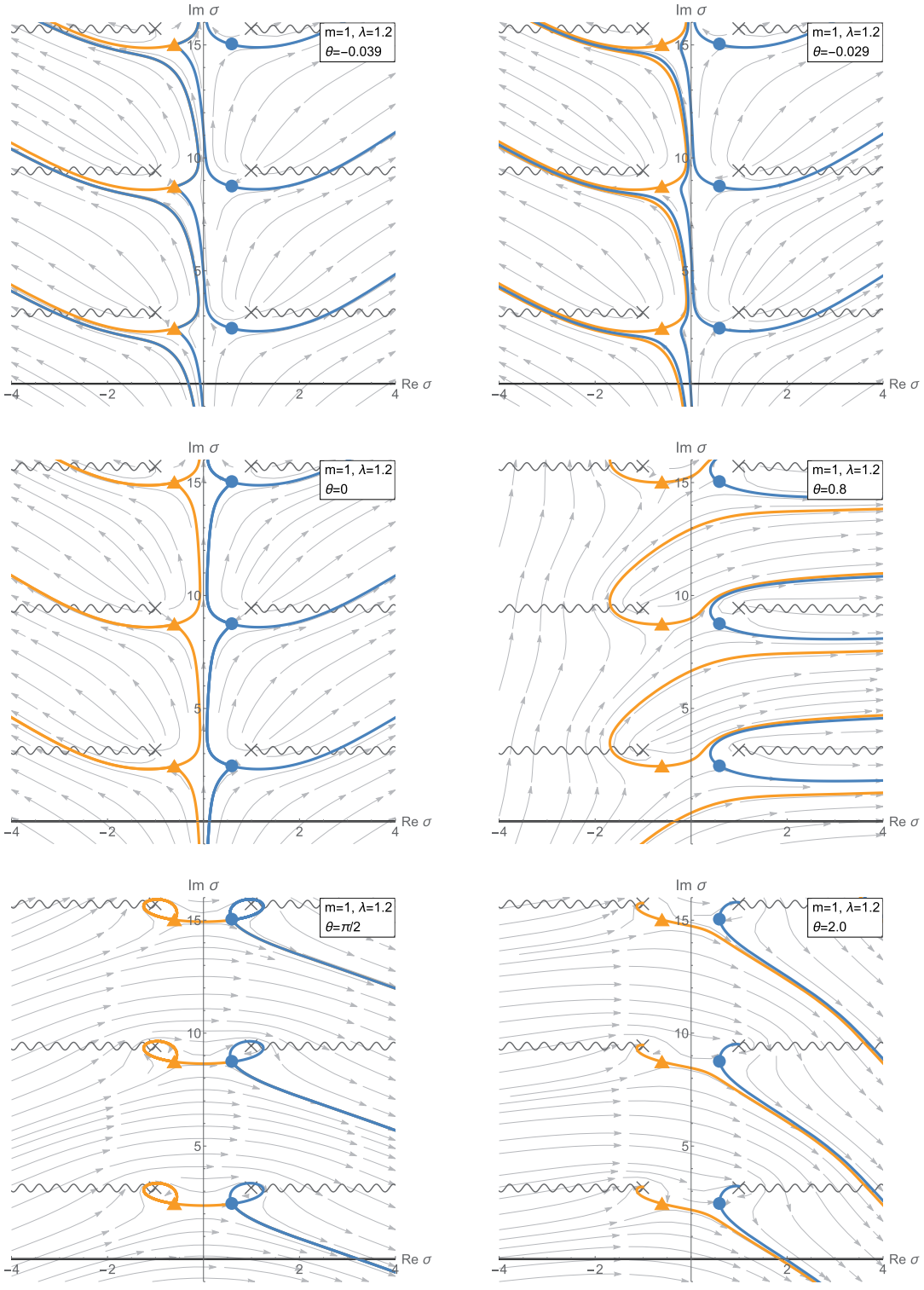

Fig. B.2. Continued.

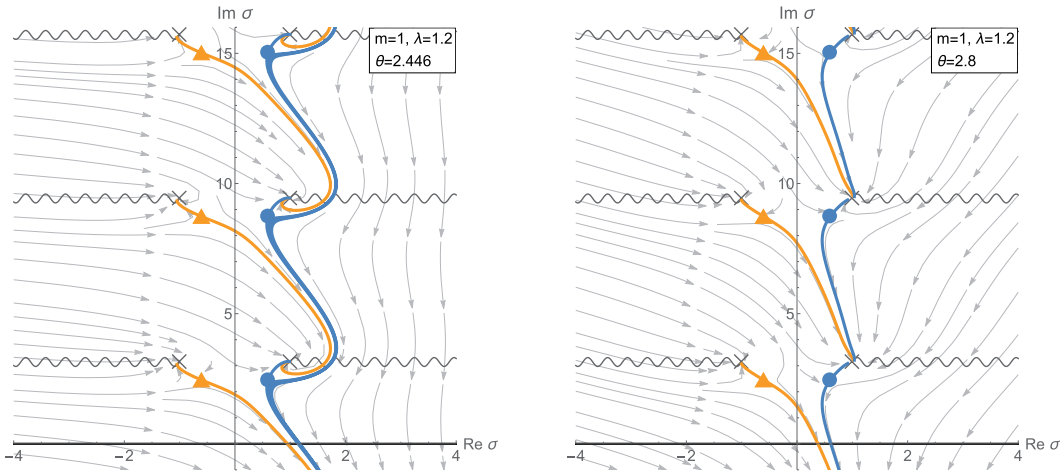

Fig. B.2. Continued.

Appendix C. Comments on the Padé-Uniformized approximation

In the main text we saw that the Padé approximation becomes worse due to branch cuts. The branch cut singularities were associated with a saddle σ_0^- in both the subcritical and supercritical regions. To make matters worse, there are other signs of branch cuts on the Borel t-plane. Figure C.1 is an example. We set $m = 10$ (for which $\lambda_c = 9.0 \times 10^{-5}$) so that singularities gather around the origin and the Padé approximation works better. We can see signs of branch cuts associated not only with a saddle σ_0^- but also with four other saddles $\sigma_{\pm 1}^{\pm}$. We claim that even the Padé-Uniformized approximation is obstructed by these branch cuts. In this appendix we discuss this point by studying some simple examples of applications of the Padé-Uniformized approximation.

Appendix C.1. Single branch cut

Let us start with the simplest case. Consider, for example, a function which has a single branch cut,

$$\mathcal{B}F(t) = \frac{1}{(1-t)^{1/5}}, \tag{C.1}$$

and a uniformization map

$$u = \psi(t) = -\ln(1-t). \tag{C.2}$$

In Fig. C.2 we compare the standard Padé approximation with the Padé-Uniformized approximation for this example. We see that the Padé-Uniformized approximation works well in this case.

Appendix C.2. Multiple branch cuts

Next let us consider the following example with two branch cuts:

$$\mathcal{B}F(t) = \frac{1}{(1-t)^{1/5}(1+t)^{1/5}}. \tag{C.3}$$

The result is shown in Fig. C.3. We see that the approximation becomes worse. In the Padé-Uniformized approximation (right panel) we can see that there is a pair of singularities above and below the negative real axis. This is an artifact due to the uniformization map, as explained below.

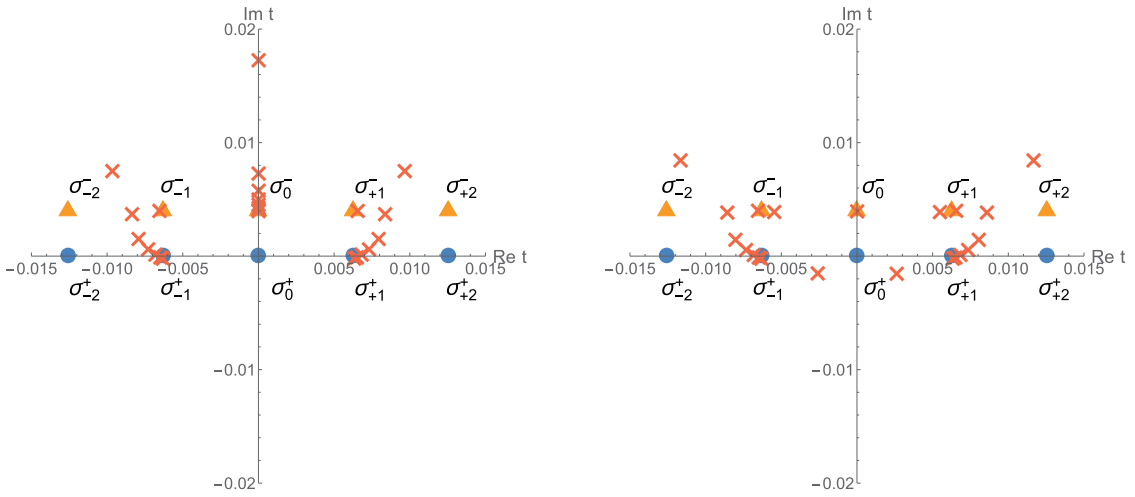

Fig. C.1. Illustrations of the Borel plane structure for the supercritical region. In this figure we set $m = 10$ and $\lambda = 1.0 \times 10^{-3} \geq \lambda_c = 9.0 \times 10^{-5}$. The left panel is obtained by the Padé approximation, and the right panel by the Padé-Uniformized approximation.

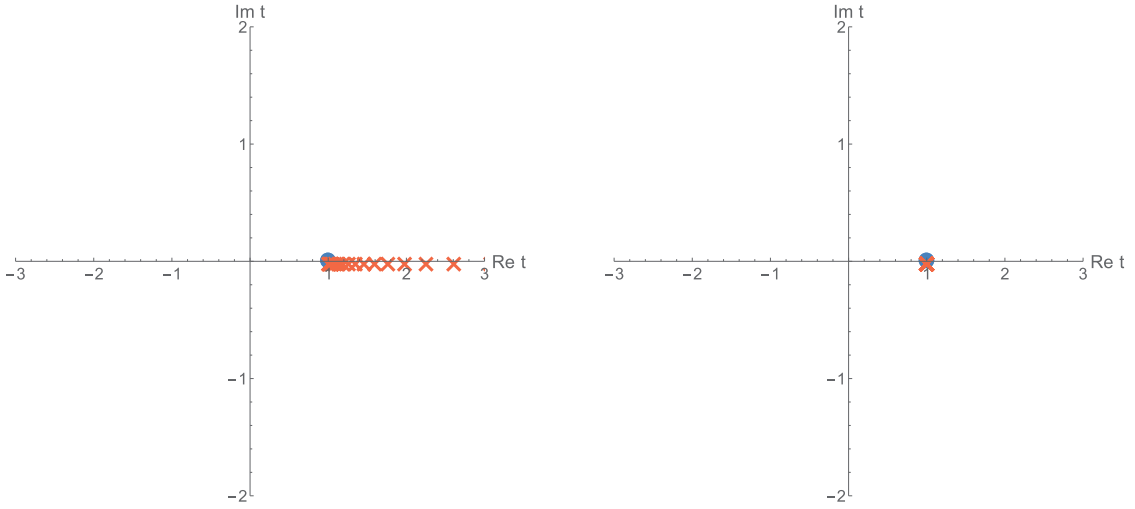

Fig. C.2. Comparison of the Padé and the Padé-Uniformized approximations (25,25) in the case of a single branch cut. Left: The Padé approximation. Right: The Padé-Uniformized approximation, where the branch cut is removed by the uniformization map.

The nth Riemann sheet of the Borel t-plane is sent to the region

$$-n\pi < \Im u < +n\pi \tag{C.4}$$

by the uniformization map. The branch cut which starts from the singularity $t = -1$ is sent to

$$\Re u < -\ln 2, \qquad \Im u = 2\pi n. \tag{C.5}$$

Then, the Padé-Uniformized approximation on the t-plane (or the standard Padé approximation on the u-plane) resembles singularities at

$$u = -\ln 2 + 2\pi i n. \tag{C.6}$$

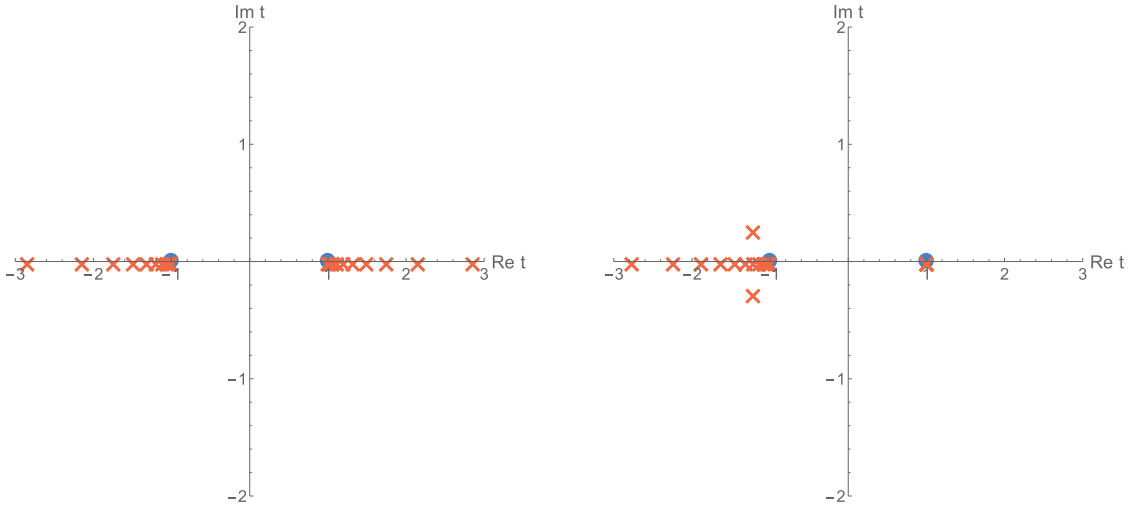

Fig. C.3. Comparison of the Padé and the Padé-Uniformized approximation (25,25) in the case with two branch cuts. One of the branch cuts is removed by the uniformization map.

Ideally, all of these are sent back to the same point $t = -1$ by the inverse map,

$$t = \phi(u) = 1 - e^{-u}. \tag{C.7}$$

However, since the approximation becomes worse away from the origin $u = 0$, the singularities found (particularly with $|n| > 0$) are not sent back exactly to $t = -1$. As a result, the Padé-Uniformized approximation returns multiple singularities around $t = -1$. The pair of singularities in the right panel of Fig. C.3 corresponds to $n = \pm 1$. Other pairs of singularities corresponding to larger $|n|$ are missing simply because they are too far away from the origin $u = 0$.

Such artifacts cause trouble since they are indistinguishable from other genuine singularities. Let us consider, for example, the function

$$\mathcal{B}F(t) = \frac{1}{(1-t)^{1/5}(1+t)^{1/5}} \frac{1}{(i-t)(i+t)}. \tag{C.8}$$

The result of the Padé(-Uniformized) approximation is shown in Fig. C.4. The two poles $t = \pm i$ are sent to

$$u = -\ln(1 \mp i), \tag{C.9}$$

while the branch cut singularities $t = \pm 1$ are sent to

$$u = -\ln 2 + 2\pi i n. \tag{C.10}$$

These two singularities $u = -\ln 2 + 2\pi i n$ are further away from the poles $u = -\ln(1 \mp i)$. Then, the approximation for the two singularities is disturbed by the poles. As a result, the Padé-Uniformized approximation returns the poles which originate in $t = \pm i$, but with much worse artifacts which originate in $t = \pm 1$. Indeed, in the right panel of Fig. C.4 the pair of artifacts is indistinguishable from the genuine poles. We claim that some of the singularities found in Sect. 4.1 are these types of artifact.

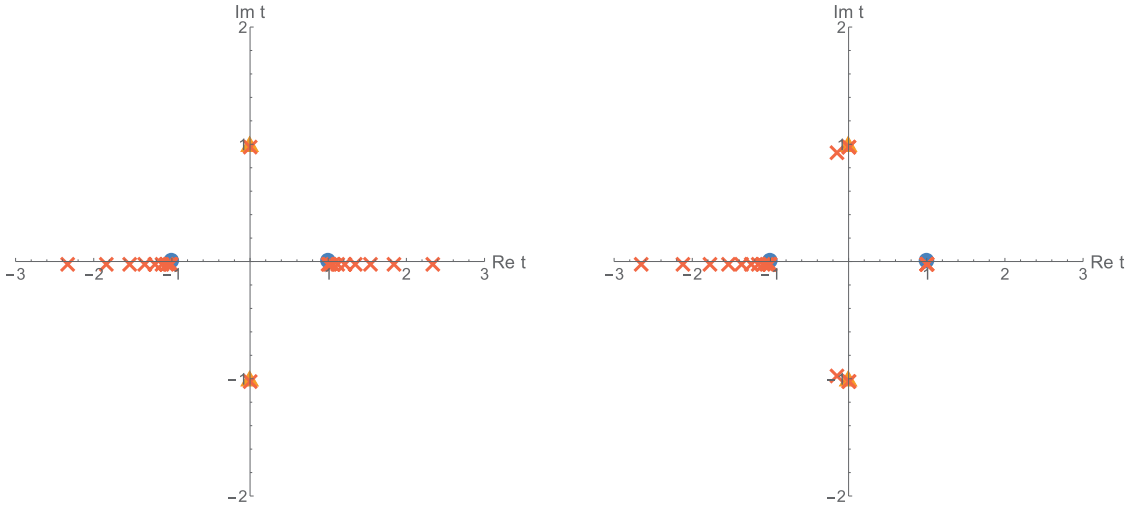

Fig. C.4. Comparison of the Padé and the Padé-Uniformized approximation (25,25) in the case of two branch cuts and two poles. One of the branch cuts is removed by the uniformization map.

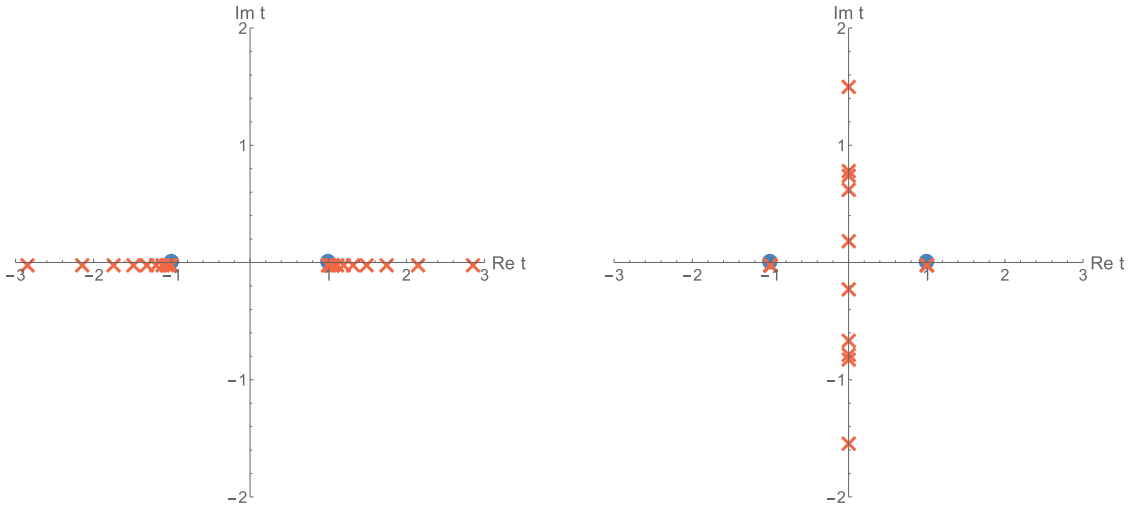

Fig. C.5. Comparison of the Padé and the Padé-Uniformized approximation (25,25) in the case of two branch cuts. The two singularities $t = \pm 1$ are mapped to $u = \pm\infty$. The multiple branch cuts are eliminated by the map.

Appendix C.3. On elimination of multiple branch cuts

One possible way to avoid such multiple branch cuts is to consider the map

$$u = \psi(t) = -\ln(1-t) + \ln(1+t), \tag{C.11}$$

which sends the singularities at $t = \pm 1$ to $u = \pm\infty$. However, this map causes other branch cuts on the u-plane. As a result, the Padé-Uniformized approximation returns a lot of artifacts along the imaginary axis, as shown in Fig. C.5. It seems that the problem resides in the non-trivial topology of the Borel t-plane due to multiple branch cuts.

For the above reasons, the multiple branch cuts worsen the Padé-Uniformized approximation. Some artifacts are indistinguishable from other genuine singularities. Also, multiple branch cuts are not

eliminated simultaneously, at least by naive maps. Further improvements of the Padé-Uniformized approximation are left for future work.

Appendix D. Transseries for finite η

In this appendix we derive the transseries for finite η from the viewpoint of a difference equation. See Refs. [2,170] for the technical details. We consider the formal transseries satisfying the difference equation ($x = N_f$)

$$Z(x+1) = f(x)Z(x) + g(x)Z(x-1), \tag{D.1}$$

where

$$f(x) = \frac{(2x-1)\cosh(m)}{2x\sinh^2(m)}, \qquad g(x) = -\frac{(x-1)^2+\eta^2}{4x(x-1)\sinh^2(m)}. \tag{D.2}$$

We introduce $P(x) = Z(x-1)$, and Eq. (D.1) can be written as a vectorial expression:

$$\mathbf{Z}(x+1) = M(x)\mathbf{Z}(x), \tag{D.3}$$

where $\mathbf{Z}(x) = (Z(x), P(x))^\top$, and the 2×2 matrix $M(x)$ is defined as

$$M(x) = \begin{pmatrix} f(x) & g(x) \\ 1 & 0 \end{pmatrix} \sim \Lambda\left(\mathbb{I} + x^{-1}A\right) + O(x^{-2}), \tag{D.4}$$

$$\Lambda = \begin{pmatrix} \frac{\cosh(m)}{\sinh^2(m)} & -\frac{1}{4\sinh^2(m)} \\ 1 & 0 \end{pmatrix}, \qquad A = \begin{pmatrix} 0 & 0 \\ 2\cosh(m) & -1 \end{pmatrix}. \tag{D.5}$$

The transseries structure generally depends on the form of the difference equation and is uniquely determined from the change of asymptotic series by acting the shift operator (see App. D.1 for details). In order to obtain the transseries based on the difference equation, one needs to diagonalize Λ and A. By using an invertible matrix U to diagonalize Λ, one finds that

$$\hat{\Lambda} = U\Lambda U^{-1} =: \mathrm{diag}(\lambda_-, \lambda_+), \tag{D.6}$$

$$\lambda_\pm = \frac{\cosh(m)\pm 1}{2\sinh^2(m)} = \frac{1}{2(\cosh(m)\mp 1)}, \tag{D.7}$$

$$\tilde{A} := UAU^{-1} = \begin{pmatrix} -\frac{1}{2} & -\frac{1}{2} + \frac{\cosh(m)}{\cosh(m)-1} \\ -\frac{1}{2} + \frac{\cosh(m)}{\cosh(m)+1} & -\frac{1}{2} \end{pmatrix}, \tag{D.8}$$

$$U = \begin{pmatrix} -\sinh^2(m) & \frac{1}{2} + \frac{\cosh(m)}{2} \\ \sinh^2(m) & \frac{1}{2} - \frac{\cosh(m)}{2} \end{pmatrix}, \tag{D.9}$$

$$\Rightarrow \quad \tilde{\mathbf{Z}}(x+1) = \tilde{M}(x)\tilde{\mathbf{Z}}(x), \tag{D.10}$$

where $\tilde{M}(x) := UM(x)U^{-1}$ and $\tilde{\mathbf{Z}}(x) := U\mathbf{Z}(x)$. Next, we consider the diagonalization for $\tilde{A}$ by employing the technique in App. D.2. In order to do so we act $W(x)$ from the left as

$$\check{\mathbf{Z}}(x+1) = \check{M}(x)\check{\mathbf{Z}}(x), \qquad \check{\mathbf{Z}}(x) := W(x)\tilde{\mathbf{Z}}(x), \tag{D.11}$$

where

$$\check{M}(x) = W(x+1)\tilde{M}(x)W^{-1}(x), \qquad W(x) := \mathbb{I} + x^{-1}V, \tag{D.12}$$

and

$$\mathrm{diag}_M[\tilde{A}] =: \mathrm{diag}(a_-, a_+), \qquad a_\pm = -\frac{1}{2}. \tag{D.13}$$

Hence,

$$Z(x) = \sum_{s=\{+,-\}} \sum_{n=0}^{\infty} \sigma_s c_{s,n} e^{\log \lambda_s \cdot x} x^{a_s - n}, \tag{D.14}$$

where the transseries in terms of x is completely determined, but is not for other parameters such as m and η. Hence, $\sigma_s = \sigma(m,\eta)$ and $c_{s,n} = c_{s,n}(m,\eta)$ in general. Since $c_{\pm,0}$ is relevant only to the normalization, one can take $c_{\pm,0} = 1$ without loss of generality. $\sigma_\pm$ can be determined from the partition function, and are given by

$$\sigma_+(m,\eta) = 0, \qquad \sigma_-(m,\eta) = \sqrt{2\pi(1+\cosh m)}. \tag{D.15}$$

Notice that $c_{\pm,n>0}$ are recursively determined from the difference equation.

Appendix D.1. Properties of the shift operator T

We define the shift operator T as $T[f(x)] = f(x+1)$. It satisfies the following homomorphic properties for summation and multiplication:

$$T[f(x) + g(x)] = T[f(x)] + T[g(x)], \tag{D.16}$$

$$T[f(x) \cdot g(x)] = T[f(x)] \cdot T[g(x)]. \tag{D.17}$$

The action of T to transmonomials gives

$$T[x^{-1}] = \frac{1}{x+1} = \sum_{n=0}^{\infty} (-1)^n x^{-1-n}, \tag{D.18}$$

$$T[x^a] = (x+1)^a = x^a (1+x^{-1})^a = x^a \sum_{n=0}^{\infty} \frac{a \cdot (a-1) \cdots (a-n+1)}{n!} x^{-n}, \tag{D.19}$$

$$T[e^{-\mu x}] = e^{-\mu(x+1)} = e^{-\mu} \cdot e^{-\mu x}, \tag{D.20}$$

$$T[\log(x)] = \log(x+1) = \log(x) + \log(1+x^{-1}) = \log(x) + \sum_{n=1}^{\infty} \frac{(-1)^{n+1} x^{-n}}{n}. \tag{D.21}$$

Notice that when $g(x+1) = g(x)$, the action of T to $g(x)$ gives the identity map. As one can see easily, for example, the below type of transseries is closed under the action of the shift operator T:

$$\sum_{n,k=0}^{\infty} e^{-n \log \mu} c_{n,k} x^{a-k} \xrightarrow{T} \sum_{n,k=0}^{\infty} e^{-n \log \mu} c'_{n,k} x^{a-k}. \tag{D.22}$$

The type of transseries and the propagation of integration constants are determined by the form of the difference equation such as (non)linearity, (non)autonomous, and so on.

Appendix D.2. Diagonalization of $M(x)$

Suppose $f(x)$ is a transseries determined by a difference equation having the form $f(x+1) = M(x)f(x)$, where $M(x)$ is a function satisfying $M(x) \sim \Lambda(1+x^{-1}A)+O(x^{-2})$ with constant Λ and A. Assume that Λ is positive. If the transseries includes $e^{-\mu x}x^a$, since the action of T gives

$$T[e^{-\mu x}x^a] = e^{-\mu}\cdot e^{-\mu x}x^a\left(1+ax^{-1}+O(x^{-2})\right), \tag{D.23}$$

μ and a are determined from Λ and A, respectively, as

$$\mu = -\log(\Lambda), \qquad a = A. \tag{D.24}$$

We can extend $f(x)$ to multi-variables, $\mathbf{f}(x) = (f_1(x),\dots,f_N(x))^\top$,

$$\mathbf{f}(x+1) = M(x)\mathbf{f}(x), \tag{D.25}$$

where $M(x)$ is an $N\times N$ matrix given by

$$M(x) = \Lambda\left(\mathbb{I}+x^{-1}A\right)+O(x^{-2}), \tag{D.26}$$

with constants matrix Λ and A. Assume that Λ is diagonalizable by an invertible matrix U and that all the eigenvalues are positive. By acting U from the left on both sides, one can obtain that

$$\tilde{\mathbf{f}}(x+1) = \tilde{M}(x)\tilde{\mathbf{f}}(x), \tag{D.27}$$

where

$$\tilde{M}(x) = \hat{\Lambda}\left(\mathbb{I}+x^{-1}\tilde{A}\right)+O(x^{-2}), \tag{D.28}$$

$$\hat{\Lambda} = U\Lambda U^{-1} =: \mathrm{diag}(\lambda_1,\dots,\lambda_N), \tag{D.29}$$

$$\tilde{A} = UAU^{-1}. \tag{D.30}$$

In order to diagonalize $\hat{\Lambda}\tilde{A}$, we redefine $\tilde{\mathbf{f}}(x)$ and the difference equation as

$$\check{\mathbf{f}}(x+1) = \check{M}(x)\check{\mathbf{f}}(x), \tag{D.31}$$

$$\check{\mathbf{f}}(x) = W(x)\tilde{\mathbf{f}}(x), \tag{D.32}$$

$$W(x) = \mathbb{I}+x^{-1}V, \tag{D.33}$$

with an $N\times N$ constant matrix V and $\check{M}(x)$ given by

$$\begin{aligned}\check{M}(x) &= W(x+1)\tilde{M}(x)W^{-1}(x)\\ &= \left(\mathbb{I}+(x+1)^{-1}V\right)\tilde{M}(x)\left(\mathbb{I}+x^{-1}V\right)^{-1}\\ &\sim \hat{\Lambda}+x^{-1}\left([V,\hat{\Lambda}]+\hat{\Lambda}\tilde{A}\right)+O(x^{-2}),\end{aligned} \tag{D.34}$$

where $[A,B] := AB-BA$. Notice that all the diagonal parts of V can be taken as zero and one can determine other $N(N-1)$-components of V such that

$$[V,\hat{\Lambda}]+\hat{\Lambda}\tilde{A} = \mathrm{diag}_M[\hat{\Lambda}\tilde{A}] = \hat{\Lambda}\,\mathrm{diag}_M[\tilde{A}], \tag{D.35}$$

$$\mathrm{diag}_M[\tilde{A}] =: \mathrm{diag}(a_1,\dots,a_N), \tag{D.36}$$

where $\mathrm{diag}_M[\tilde{A}]$ is a diagonal matrix having diagonal parts of $\tilde{A}$.

Appendix E. Transseries for a finite $\lambda = \eta/N_f$

Let us rewrite the recursion relation in Eq. (D.1) in terms of a fixed $\lambda = \eta/N_f$:

$$Z(x+1) = f(x)Z(x) + g(x)Z(x-1), \tag{E.1}$$

where

$$f(x) = \frac{(2x-1)\cosh(m)}{2x\sinh^2(m)}, \qquad g(x) = -\frac{(x-1)^2 + x^2\lambda^2}{4x(x-1)\sinh^2(m)}. \tag{E.2}$$

If we ignore the extra dependence of $Z(x,\eta)$ on x through $\eta = \lambda/x$, we find that the vectorial recursion relation for $\mathbf{Z}(x) = (Z(x), P(x))^\top$ is modified to

$$\mathbf{Z}(x+1) = M(x)\mathbf{Z}(x), \tag{E.3}$$

$$M(x) = \begin{pmatrix} f(x) & g(x) \\ 1 & 0 \end{pmatrix} \sim \Gamma\left(\mathbb{I} + x^{-1}\mathcal{A}\right) + O(x^{-2}), \tag{E.4}$$

$$\Gamma = \begin{pmatrix} \frac{\cosh(m)}{\sinh^2(m)} & -\frac{\lambda^2+1}{4\sinh^2(m)} \\ 1 & 0 \end{pmatrix}, \qquad \mathcal{A} = \begin{pmatrix} 0 & 0 \\ \frac{2\cosh(m)}{\lambda^2+1} & \frac{\lambda^2-1}{\lambda^2+1} \end{pmatrix}. \tag{E.5}$$

By diagonalizing the matrix Γ, we find two exponents $\gamma_\pm$:

$$\tilde{M}(x) = \hat{\Gamma}\left(\mathbb{I} + x^{-1}\tilde{\mathcal{A}}\right) + O(x^{-2}), \tag{E.6}$$

$$\hat{\Gamma} = U\Gamma U^{-1} =: \mathrm{diag}(\gamma_+, \gamma_-), \tag{E.7}$$

$$\tilde{\mathcal{A}} = U\mathcal{A}U^{-1}, \tag{E.8}$$

$$\gamma_\pm = \frac{\cosh m \pm \sqrt{1 - \lambda^2\sinh^2 m}}{2\sinh^2 m}. \tag{E.9}$$

These two exponents are degenerate when

$$\lambda = \frac{1}{\sinh m}, \tag{E.10}$$

which agrees with the critical point λ_c in Eq. (2.10) for the phase transition.

Appendix F. A possible relation between the Borel singularities and complex SUSY solutions

In this appendix we point out that a path integral interpretation of the Borel singularities appearing in the main text may be complex supersymmetric solutions (CSS) as found in Ref. [115]. It was proposed that Borel transformation of large Chern–Simons level expansion include the factor

$$\mathcal{B}Z(t) \supset \prod_{\mathrm{CSS}} \frac{1}{(t - S_c)^{n_B - n_F}}, \tag{F.1}$$

where n_B (n_F) is the number of bosonic (fermionic) solutions. In the SQED studied in this paper there are two types of CSS with $n_B - n_F \neq 0$, more precisely $n_B - n_F = N_f$. Actions of the solutions are

$$S_{\mathrm{CSS}} = N_f(2\pi n\lambda \mp i\lambda m), \tag{F.2}$$

while the action at the saddle points $\sigma_n^{\pm}$ in the localization formula is

$$S_n^{\pm} = N_f \left[2\pi n\lambda - \frac{i\lambda}{2} \log \frac{(-\lambda \cosh m \mp i\Delta)(-i+\lambda)}{(-\lambda \cosh m \pm i\Delta)(i+\lambda)} + \log \frac{\cosh m \pm \Delta}{1+\lambda^2} \right]. \tag{F.3}$$

Comparing this with Eq. (F.2), we find that these actions agree when λ is large ($\lambda \gg 1$). Thus, it seems plausible that the Borel singularities correspond to the CSS in the original path integral, at least for large λ. It would be interesting to extend the analysis in this appendix to finite λ.

References

[1] J. Ecalle, *Les Fonctions Resurgentes* (Université de Paris-Sud, Paris, 1981) Vols. I–III.
[2] O. Costin, *Asymptotics and Borel Summability* (CRC Press, Hoboken, NJ, 2008).
[3] M. Mariño, Fortsch. Phys. **62**, 455 (2014) [arXiv:1206.6272 [hep-th]] [Search INSPIRE].
[4] D. Dorigoni, Ann. Phys. **409**, 167914 (2019) [arXiv:1411.3585 [hep-th]] [Search INSPIRE].
[5] I. Aniceto, G. Başar, and R. Schiappa, Phys. Rept. **809**, 1 (2019) [arXiv:1802.10441 [hep-th]] [Search INSPIRE].
[6] D. Sauzin, arXiv:1405.0356 [math.DS].
[7] C. M. Bender and T. T. Wu, Phys. Rev. **184**, 1231 (1969).
[8] C. M. Bender and T. T. Wu, Phys. Rev. D **7**, 1620 (1973).
[9] R. Balian, G. Parisi, and A. Voros, Quartic Oscillator, in *Feynman Path Integrals*, eds. S. Albeverio, Ph. Combe, R. Høegh-Krohn, G. Rideau, M. Sirugue-Collin, M. Sirugue, and R. Stora (Springer, New York, 1979), p. 337.
[10] A. Voros, *Ann. Inst. Henri Poincaré Phys. Théor.* **39**, 211 (1983).
[11] J. Zinn-Justin and U. D. Jentschura, Ann. Phys. **313**, 197 (2004) [arXiv:quant-ph/0501136] [Search INSPIRE].
[12] J. Zinn-Justin and U. D. Jentschura, Ann. Phys. **313**, 269 (2004) [arXiv:quant-ph/0501137] [Search INSPIRE].
[13] U. D. Jentschura, A. Surzhykov, and J. Zinn-Justin, Ann. Phys. **325**, 1135 (2010) [arXiv:1001.3910 [math-ph]] [Search INSPIRE].
[14] U. D. Jentschura and J. Zinn-Justin, Ann. Phys. **326**, 2186 (2011).
[15] G. V. Dunne and M. Ünsal, Phys. Rev. D **89**, 041701(R) (2014) [arXiv:1306.4405 [hep-th]] [Search INSPIRE].
[16] G. Basar, G. V. Dunne, and M. Ünsal, J. High Energy Phys. **1310**, 041 (2013) [arXiv:1308.1108 [hep-th]] [Search INSPIRE].
[17] G. V. Dunne and M. Ünsal, Phys. Rev. D **89**, 105009(R) (2014) [arXiv:1401.5202 [hep-th]] [Search INSPIRE].
[18] M. A. Escobar-Ruiz, E. Shuryak, and A. V. Turbiner, Phys. Rev. D **92**, 025046 (2015); **92**, 089902 (2015) [erratum] [arXiv:1501.03993 [hep-th]] [Search INSPIRE].
[19] M. A. Escobar-Ruiz, E. Shuryak, and A. V. Turbiner, Phys. Rev. D **92**, 025047 (2015) [arXiv:1505.05115 [hep-th]] [Search INSPIRE].
[20] T. Misumi, M. Nitta, and N. Sakai, J. High Energy Phys. **1509**, 157 (2015) [arXiv:1507.00408 [hep-th]] [Search INSPIRE].
[21] A. Behtash, G. V. Dunne, T. Schäfer, T. Sulejmanpasic, and M. Ünsal, Phys. Rev. Lett. **116**, 011601 (2016) [arXiv:1510.00978 [hep-th]] [Search INSPIRE].
[22] A. Behtash, G. V. Dunne, T. Schäfer, T. Sulejmanpasic, and M. Ünsal, Ann. Math. Sci. Appl. **2**, 95 (2017) [arXiv:1510.03435 [hep-th]] [Search INSPIRE].
[23] I. Gahramanov and K. Tezgin, Phys. Rev. D **93**, 065037 (2016) [arXiv:1512.08466 [hep-th]] [Search INSPIRE].
[24] G. V. Dunne and M. Unsal, arXiv:1603.04924 [math-ph] [Search INSPIRE].
[25] C. Kozçaz, T. Sulejmanpasic, Y. Tanizaki, and M. Ünsal, Commun. Math. Phys. **364**, 835 (2018) [arXiv:1609.06198 [hep-th]] [Search INSPIRE].
[26] T. Fujimori, S. Kamata, T. Misumi, M. Nitta, and N. Sakai, Phys. Rev. D **94**, 105002 (2016) [arXiv:1607.04205 [hep-th]] [Search INSPIRE].
[27] G. V. Dunne and M. Ünsal, J. High Energy Phys. **1612**, 002 (2016) [arXiv:1609.05770 [hep-th]] [Search INSPIRE].

[28] M. Serone, G. Spada, and G. Villadoro, Phys. Rev. D **96**, 021701(R) (2017) [arXiv:1612.04376 [hep-th]] [Search INSPIRE].
[29] G. Basar, G. V. Dunne, and M. Ünsal, J. High Energy Phys. **1705**, 087 (2017) [arXiv:1701.06572 [hep-th]] [Search INSPIRE].
[30] G. Álvarez and H. J. Silverstone, J. Phys. Comm. **1**, 025005 (2017) [arXiv:1706.00329 [math-ph]] [Search INSPIRE].
[31] A. Behtash, G. V. Dunne, T. Schäfer, T. Sulejmanpasic, and M. Ünsal, J. High Energy Phys. **1806**, 068 (2018) arXiv:1803.11533 [hep-th]] [Search INSPIRE].
[32] Z. Duan, J. Gu, Y. Hatsuda, and T. Sulejmanpasic, J. High Energy Phys. **1901**, 079 (2019) [arXiv:1806.11092 [hep-th]] [Search INSPIRE].
[33] M. Raman and P. N. Bala Subramanian, Phys. Rev. D **101**, 126014 (2020) [arXiv:2002.01794 [hep-th]] [Search INSPIRE].
[34] N. Sueishi, Prog. Theor. Exp. Phys. **2021**, 013B01 (2021) [arXiv:1912.03518 [hep-th]] [Search INSPIRE].
[35] N. Sueishi, S. Kamata, T. Misumi, and M. Ünsal, J. High Energy Phys. **2012**, 114 (2020) [arXiv:2008.00379 [hep-th]] [Search INSPIRE].
[36] N. Sueishi, S. Kamata, T. Misumi, and M. Ünsal, arXiv:2103.06586 [quant-ph] [Search INSPIRE].
[37] I. Aniceto and M. Spaliński, Phys. Rev. D **93**, 085008 (2016) [arXiv:1511.06358 [hep-th]] [Search INSPIRE].
[38] G. Başar and G. V. Dunne, Phys. Rev. D **92**, 125011 (2015) [arXiv:1509.05046 [hep-th]] [Search INSPIRE].
[39] J. Casalderrey-Solana, N. I. Gushterov, and B. Meiring, J. High Energy Phys. **1804**, 042 (2018) [arXiv:1712.02772 [hep-th]] [Search INSPIRE].
[40] A. Behtash, C. N. Cruz-Camacho, and M. Martinez, Phys. Rev. D **97**, 044041 (2018) [arXiv:1711.01745 [hep-th]] [Search INSPIRE].
[41] M. P. Heller and V. Svensson, Phys. Rev. D **98**, 054016 (2018) [arXiv:1802.08225 [nucl-th]] [Search INSPIRE].
[42] M. P. Heller, A. Serantes, M. Spaliński, V. Svensson, and B. Withers, arXiv:2007.05524 [hep-th] [Search INSPIRE].
[43] I. Aniceto, J. Jankowski, B. Meiring, and M. Spaliński, J. High Energy Phys. **1902**, 073 (2019) [arXiv:1810.07130 [hep-th]] [Search INSPIRE].
[44] A. Behtash, S. Kamata, M. Martinez, T. Schäfer, and V. Skokov, Phys. Rev. D **103**, 056010 (2021) [arXiv:2011.08235 [hep-ph]] [Search INSPIRE].
[45] K. Ito, M. Mariño, and H. Shu, J. High Energy Phys. **1901**, 228 (2019) [arXiv:1811.04812 [hep-th]] [Search INSPIRE].
[46] L. Schepers and D. C. Thompson, Nucl. Phys. B **964**, 115308 (2021) [arXiv:2007.03683 [hep-th]] [Search INSPIRE].
[47] M. Mariño and T. Reis, arXiv:1905.09569 [hep-th] [Search INSPIRE].
[48] M. Mariño and T. Reis, J. High Energy Phys. **2004**, 160 (2020) [arXiv:1909.12134 [hep-th]] [Search INSPIRE].
[49] M. Mariño and T. Reis, J. High Energy Phys. **2007**, 216 (2020) [arXiv:1912.06228 [hep-th]] [Search INSPIRE].
[50] M. Marino and T. Reis, arXiv:2006.05131 [hep-th] [Search INSPIRE].
[51] M. Marino and T. Reis, arXiv:2010.16174 [hep-th] [Search INSPIRE].
[52] M. Marino, R. M. Mas, and T. Reis, [arXiv:2102.03078 [hep-th] [Search INSPIRE].
[53] M. Mariño, R. Schiappa, and M. Weiss, J. Math. Phys. **50**, 052301 (2009) [arXiv:0809.2619 [hep-th]] [Search INSPIRE].
[54] S. Garoufalidis, A. Its, A. Kapaev, and M. Mariño, Int. Math. Res. Not. **2012**, 561 (2012) [arXiv:1002.3634 [math.CA]] [Search INSPIRE].
[55] C.-T. Chan, H. Irie, and C.-H. Yeh, Nucl. Phys. B **854**, 67 (2012) [arXiv:1011.5745 [hep-th]] [Search INSPIRE].
[56] C.-T. Chan, H. Irie, and C.-H. Yeh, Nucl. Phys. B **855**, 46 (2012) [arXiv:1109.2598 [hep-th]] [Search INSPIRE].
[57] R. Schiappa and R. Vaz, Commun. Math. Phys. **330**, 655 (2014) [arXiv:1302.5138 [hep-th]] [Search INSPIRE].
[58] M. Mariño, J. High Energy Phys. **0803**, 060 (2008) [arXiv:hep-th/0612127] [Search INSPIRE].

[59] M. Mariño, R. Schiappa, and M. Weiss, Commun. Num. Theor. Phys. **2**, 349 (2008) [arXiv:0711.1954 [hep-th]] [Search INSPIRE].
[60] M. Mariño, J. High Energy Phys. **0812**, 114 (2008) [arXiv:0805.3033 [hep-th]] [Search INSPIRE].
[61] S. Pasquetti and R. Schiappa, Ann. Henri Poincaré **11**, 351 (2010) [arXiv:0907.4082 [hep-th]] [Search INSPIRE].
[62] I. Aniceto, R. Schiappa, and M. Vonk, Commun. Num. Theor. Phys. **6**, 339 (2012) [arXiv:1106.5922 [hep-th]] [Search INSPIRE].
[63] R. Couso-Santamaría, J. D. Edelstein, R. Schiappa, and M. Vonk, Ann. Henri Poincaré **17**, 331 (2016) [arXiv:1308.1695 [hep-th]] [Search INSPIRE].
[64] R. Couso-Santamaría, J. D. Edelstein, R. Schiappa, and M. Vonk, Commun. Math. Phys. **338**, 285 (2015) [arXiv:1407.4821 [hep-th]] [Search INSPIRE].
[65] A. Grassi, M. Mariño, and S. Zakany, J. High Energy Phys. **1505**, 038 (2015) [arXiv:1405.4214 [hep-th]] [Search INSPIRE].
[66] R. Couso-Santamaría, R. Schiappa, and R. Vaz, Ann. Phys. **356**, 1 (2015) [arXiv:1501.01007 [hep-th] [Search INSPIRE].
[67] R. Couso-Santamaría, R. Schiappa, and R. Vaz, Commun. Num. Theor. Phys. **11**, 707 (2017) [arXiv:1605.07473 [math.AG]] [Search INSPIRE].
[68] R. Couso-Santamaría, M. Mariño, and R. Schiappa, J. Phys. A: Math. Theor. **50**, 145402 (2017) [arXiv:1610.06782 [hep-th]] [Search INSPIRE].
[69] T. Kuroki and F. Sugino, J. High Energy Phys. **1905**, 138 (2019) [arXiv:1901.10349 [hep-th]] [Search INSPIRE].
[70] T. Kuroki, J. High Energy Phys. **2007**, 118 (2020) [arXiv:2004.13346 [hep-th]] [Search INSPIRE].
[71] D. Dorigoni and A. Kleinschmidt, Commun. Num. Theor. Phys. **15**, 1 (2021) [arXiv:2001.11035 [hep-th]] [Search INSPIRE].
[72] G. V. Dunne and M. Ünsal, J. High Energy Phys. **1211**, 170 (2012) [arXiv:1210.2423 [hep-th]] [Search INSPIRE].
[73] G. V. Dunne and M. Ünsal, Phys. Rev. D **87**, 025015 (2013) [arXiv:1210.3646 [hep-th]] [Search INSPIRE].
[74] A. Cherman, D. Dorigoni, G. V. Dunne, and M. Ünsal, Phys. Rev. Lett. **112**, 021601 (2014) [arXiv:1308.0127 [hep-th]] [Search INSPIRE].
[75] A. Cherman, D. Dorigoni, and M. Ünsal, J. High Energy Phys. **1510**, 056 (2015) [arXiv:1403.1277 [hep-th]] [Search INSPIRE].
[76] T. Misumi, M. Nitta, and N. Sakai, J. High Energy Phys. **1406**, 164 (2014) [arXiv:1404.7225 [hep-th]] [Search INSPIRE].
[77] M. Nitta, J. High Energy Phys. **1503**, 108 (2015) [arXiv:1412.7681 [hep-th]] [Search INSPIRE].
[78] M. Nitta, J. High Energy Phys. **1508**, 063 (2015) [arXiv:1503.06336 [hep-th]] [Search INSPIRE].
[79] A. Behtash, T. Sulejmanpasic, T. Schäfer, and M. Ünsal, Phys. Rev. Lett. **115**, 041601 (2015) [arXiv:1502.06624 [hep-th]] [Search INSPIRE].
[80] G. V. Dunne and M. Ünsal, J. High Energy Phys. **1509**, 199 (2015) [arXiv:1505.07803 [hep-th]] [Search INSPIRE].
[81] P. V. Buividovich, G. V. Dunne, and S. N. Valgushev, Phys. Rev. Lett. **116**, 132001 (2016) [arXiv:1512.09021 [hep-th]] [Search INSPIRE].
[82] S. Demulder, D. Dorigoni, and D. C. Thompson, J. High Energy Phys. **1607**, 088 (2016) [arXiv:1604.07851 [hep-th]] [Search INSPIRE].
[83] T. Sulejmanpasic, Phys. Rev. Lett. **118**, 011601 (2017).
[84] K. Okuyama and K. Sakai, J. High Energy Phys. **1808**, 065 (2018) [arXiv:1806.00189 [hep-th]] [Search INSPIRE].
[85] M. C. Abbott, Z. Bajnok, J. Balog, A. Hegedús, and S. Sadeghian, J. High Energy Phys. **2105**, 253 (2021) [arXiv:2011.12254 [hep-th]] [Search INSPIRE].
[86] M. C. Abbott, Z. Bajnok, J. Balog, and A. Hegedűs, Phys. Lett. B **818**, 136369 (2021) [arXiv:2011.09897 [hep-th]] [Search INSPIRE].
[87] K. Ishikawa, O. Morikawa, A. Nakayama, K. Shibata, H. Suzuki, and H. Takaura, Prog. Theor. Exp. Phys. **2020**, 023B10 (2020) [arXiv:1908.00373 [hep-th]] [Search INSPIRE].
[88] K. Ishikawa, M. Okuto, K. Shibata, and H. Suzuki, Prog. Theor. Exp. Phys. **2020**, 063B02 (2020) [arXiv:2001.07302 [hep-th]] [Search INSPIRE].
[89] S. Gukov, M. Marino, and P. Putrov, arXiv:1605.07615 [hep-th] [Search INSPIRE].

[90] D. Gang and Y. Hatsuda, J. High Energy Phys. **1807**, 053 (2018) [arXiv:1710.09994 [hep-th]] [Search INSPIRE].
[91] D. H. Wu, J. High Energy Phys. **2102**, 008 (2021) [arXiv:2010.13736 [hep-th]] [Search INSPIRE].
[92] S. Garoufalidis, J. Gu, and M. Marino, Commun. Math. Phys. **386**, 469 (2021) [arXiv:2007.10190 [hep-th]] [Search INSPIRE].
[93] S. Garoufalidis, J. Gu, and M. Marino, arXiv:2012.00062 [math.GT] [Search INSPIRE].
[94] H. Fuji, K. Iwaki, H. Murakami, and Y. Terashima, Commun. Math. Phys. **386**, 225 (2021) [arXiv:2007.15872 [math.GT]] [Search INSPIRE].
[95] F. Ferrari and P. Putrov, arXiv:2009.14196 [hep-th] [Search INSPIRE].
[96] S. Gukov and C. Manolescu, arXiv:1904.06057 [math.GT] [Search INSPIRE].
[97] M. Barsanti, S. Bolognesi, F. Canfora, and G. Tallarita, Eur. Phys. J. C **80**, 1201 (2020) [arXiv:2006.02394 [hep-th]] [Search INSPIRE].
[98] P. Argyres and M. Ünsal, Phys. Rev. Lett. **109**, 121601 (2012) [arXiv:1204.1661 [hep-th]] [Search INSPIRE].
[99] G. V. Dunne, M. Shifman, and M. Ünsal, Phys. Rev. Lett. **114**, 191601 (2015) [arXiv:1502.06680 [hep-th]] [Search INSPIRE].
[100] M. Yamazaki and K. Yonekura, J. High Energy Phys. **1707**, 088 (2017) [arXiv:1704.05852 [hep-th]] [Search INSPIRE].
[101] H. Mera, T. G. Pedersen, and B. K. Nikolić, Phys. Rev. D **97**, 105027 (2018) [arXiv:1802.06034 [hep-th]] [Search INSPIRE].
[102] E. Itou, J. High Energy Phys. **1905**, 093 (2019) [arXiv:1811.05708 [hep-th]] [Search INSPIRE].
[103] F. Canfora, M. Lagos, S. H. Oh, J. Oliva, and A. Vera, Phys. Rev. D **98**, 085003 (2018) [arXiv:1809.10386 [hep-th]] [Search INSPIRE].
[104] M. Ashie, O. Morikawa, H. Suzuki, H. Takaura, and K. Takeuchi, Prog. Theor. Exp. Phys. **2020**, 023B01 (2020) [arXiv:1909.05489 [hep-th]] [Search INSPIRE].
[105] K. Ishikawa, O. Morikawa, K. Shibata, H. Suzuki, and H. Takaura, Prog. Theor. Exp. Phys. **2020**, 013B01 (2020) [arXiv:1909.09579 [hep-th]] [Search INSPIRE].
[106] M. Ünsal, arXiv:2007.03880 [hep-th] [Search INSPIRE].
[107] M. Ashie, O. Morikawa, H. Suzuki, and H. Takaura, Prog. Theor. Exp. Phys. **2020**, 093B02 (2020) [arXiv:2005.07407 [hep-th]] [Search INSPIRE].
[108] O. Morikawa and H. Takaura, Phys. Lett. B **807**, 135570 (2020) [arXiv:2003.04759 [hep-th]] [Search INSPIRE].
[109] J. G. Russo, J. High Energy Phys. **1206**, 038 (2012) [arXiv:1203.5061 [hep-th]] [Search INSPIRE].
[110] I. Aniceto, J. G. Russo, and R. Schiappa, J. High Energy Phys. **1503**, 172 (2015) [arXiv:1410.5834 [hep-th]] [Search INSPIRE].
[111] I. Aniceto, J. Phys. A: Math. Theor. **49**, 065403 (2016) [arXiv:1506.03388 [hep-th]] [Search INSPIRE].
[112] M. Honda, Phys. Rev. Lett. **116**, 211601 (2016) [arXiv:1603.06207 [hep-th]] [Search INSPIRE].
[113] M. Honda, Phys. Rev. D **94**, 025039 (2016) [arXiv:1604.08653 [hep-th]] [Search INSPIRE].
[114] S. Gukov, Nucl. Phys. B **919**, 583 (2017) [arXiv:1608.06638 [hep-th]] [Search INSPIRE].
[115] M. Honda, Phys. Rev. Lett. **121**, 021601 (2018) [arXiv:1710.05010 [hep-th]] [Search INSPIRE].
[116] S. Gukov, D. Pei, P. Putrov, and C. Vafa, J. Knot Theor. Ramifications **29**, 2040003 (2020) [arXiv:1701.06567 [hep-th]] [Search INSPIRE].
[117] D. Dorigoni and P. Glass, SciPost Phys. **4**, 012 (2018) [arXiv:1711.04802 [hep-th]] [Search INSPIRE].
[118] M. Honda and D. Yokoyama, Phys. Rev. D **100**, 025012 (2019) [arXiv:1711.10799 [hep-th]] [Search INSPIRE].
[119] T. Fujimori, M. Honda, S. Kamata, T. Misumi, and N. Sakai, Prog. Theor. Exp. Phys. **2018**, 123B03 (2018) [arXiv:1805.12137 [hep-th]] [Search INSPIRE].
[120] A. Grassi, J. Gu, and M. Mariño, J. High Energy Phys. **2007**, 106 (2020) [arXiv:1908.07065 [hep-th]] [Search INSPIRE].
[121] D. Dorigoni and P. Glass, J. High Energy Phys. **1912**, 085 (2019) [arXiv:1909.05262 [hep-th]] [Search INSPIRE].
[122] D. Dorigoni, M. B. Green, and C. Wen, J. High Energ. Phys. **2105**, 089 (2021) [arXiv:2102.09537 [hep-th]] [Search INSPIRE].
[123] L. Klaczynski Ann. Phys. **372**, 397 (2016) [arXiv:1601.04140 [hep-th]] [Search INSPIRE].

[124] J. Bersini, A. Maiezza, and J. C. Vasquez, Ann. Phys. **415**, 168126 (2020) [arXiv:1910.14507 [hep-th]] [Search INSPIRE].
[125] M. P. Bellon and E. I. Russo, Lett. Math. Phys. **111**, 42 (2021) [arXiv:2011.13822 [hep-th]] [Search INSPIRE].
[126] M. Borinsky and G. V. Dunne, Nucl. Phys. B **957**, 115096 (2020) [arXiv:2005.04265 [hep-th]] [Search INSPIRE].
[127] M. P. Bellon and E. I. Russo, Lett. Math. Phys. **111**, 42 (2021) [arXiv:2007.15675 [hep-th]] [Search INSPIRE].
[128] J. Engelsöy, J. Larana-Aragon, B. Sundborg, and N. Wintergerst, J. High Energy Phys. **2009**, 103 (2020) [arXiv:2007.00589 [hep-th]] [Search INSPIRE].
[129] N. Dondi, I. Kalogerakis, D. Orlando, and S. Reffert, J. High Energ. Phys. **2105**, 035 (2021) [arXiv:2102.12488 [hep-th]] [Search INSPIRE].
[130] E. Witten, AMS/IP Stud. Adv. Math. **50**, 347 (2011) [arXiv:1001.2933 [hep-th]] [Search INSPIRE].
[131] E. Witten, arXiv:1009.6032 [hep-th] [Search INSPIRE].
[132] D. Harlow, J. Maltz, and E. Witten, J. High Energy Phys. **1112**, 071 (2011) [arXiv:1108.4417 [hep-th]] [Search INSPIRE].
[133] M. Cristoforetti, F. Di Renzo, and L. Scorzato [AuroraScience Collaboration], Phys. Rev. D **86**, 074506 (2012) [arXiv:1205.3996 [hep-lat]] [Search INSPIRE].
[134] M. Cristoforetti, F. Di Renzo, A. Mukherjee, and L. Scorzato, Phys. Rev. D **88**, 051501(R) (2013) [arXiv:1303.7204 [hep-lat]] [Search INSPIRE].
[135] H. Fujii, D. Honda, M. Kato, Y. Kikukawa, S. Komatsu, and T. Sano, J. High Energy Phys. **1310**, 147 (2013) [arXiv:1309.4371 [hep-lat]] [Search INSPIRE].
[136] A. Mukherjee, M. Cristoforetti, and L. Scorzato, Phys. Rev. D **88**, 051502(R) (2013) [arXiv:1308.0233 [physics.comp-ph]] [Search INSPIRE].
[137] G. Aarts, Phys. Rev. D **88**, 094501 (2013) [arXiv:1308.4811 [hep-lat]] [Search INSPIRE].
[138] M. Cristoforetti, F. Di Renzo, G. Eruzzi, A. Mukherjee, C. Schmidt, L. Scorzato, and C. Torrero, Phys. Rev. D **89**, 114505 (2014) [arXiv:1403.5637 [hep-lat]] [Search INSPIRE].
[139] Y. Tanizaki and T. Koike, Ann. Phys. **351**, 250 (2014) [arXiv:1406.2386 [math-ph]] [Search INSPIRE].
[140] Y. Tanizaki, H. Nishimura, and K. Kashiwa, Phys. Rev. D **91**, 101701(R) (2015) [arXiv:1504.02979 [hep-th]] [Search INSPIRE].
[141] A. Alexandru, G. Başar, P. F. Bedaque, G. W. Ridgway, and N. C. Warrington, Phys. Rev. D **95**, 014502 (2017) [arXiv:1609.01730 [hep-lat]] [Search INSPIRE].
[142] A. Alexandru, G. Başar, P. Bedaque, G. W. Ridgway, and N. C. Warrington, Phys. Rev. D **94**, 045017 (2016) [arXiv:1606.02742 [hep-lat]] [Search INSPIRE].
[143] J. G. Russo and M. Tierz, Phys. Rev. D **95**, 031901(R) (2017) [arXiv:1610.08527 [hep-th]] [Search INSPIRE].
[144] A. Mukherjee and M. Cristoforetti, Phys. Rev. B **90**, 035134 (2014) [arXiv:1403.5680 [cond-mat.str-el]] [Search INSPIRE].
[145] Y. Tanizaki, Y. Hidaka, and T. Hayata, New J. Phys. **18**, 033002 (2016) [arXiv:1509.07146 [hep-th]] [Search INSPIRE].
[146] A. Ahmed, arXiv:1802.09095 [hep-th] [Search INSPIRE].
[147] T. Kanazawa and Y. Tanizaki, J. High Energy Phys. **1503**, 044 (2015) [arXiv:1412.2802 [hep-th]] [Search INSPIRE].
[148] A. Ahmed and G. V. Dunne, J. High Energy Phys. **1711**, 054 (2017) [arXiv:1710.01812 [hep-th]] [Search INSPIRE].
[149] A. Ahmed and G. V. Dunne, Phys. Lett. B **785**, 342 (2018) [arXiv:1808.05236 [hep-th]] [Search INSPIRE].
[150] D. J. Gross and E. Witten, Phys. Rev. D **21**, 446 (1980).
[151] S. R. Wadia, Phys. Lett. B **93**, 403 (1980).
[152] G. V. Dunne, J. Phys. A: Math. Theor. **52**, 463001 (2019) [arXiv:1901.02076 [hep-th]] [Search INSPIRE].
[153] O. Costin and G. V. Dunne, J. Phys. A: Math. Theor. **52**, 445205 (2019) [arXiv:1904.11593 [hep-th]] [Search INSPIRE].
[154] V. Pestun, Commun. Math. Phys. **313**, 71 (2012) [arXiv:0712.2824 [hep-th]] [Search INSPIRE].
[155] A. Kapustin, B. Willett, and I. Yaakov, J. High Energy Phys. **1003**, 089 (2010) [arXiv:0909.4559 [hep-th]] [Search INSPIRE].

[156] N. Hama, K. Hosomichi, and S. Lee, J. High Energy Phys. **1103**, 127 (2011) [arXiv:1012.3512 [hep-th]] [Search INSPIRE].
[157] D. L. Jafferis, J. High Energy Phys. **1205**, 159 (2012) [arXiv:1012.3210 [hep-th]] [Search INSPIRE].
[158] M. V. Berry and C. J. Howls, Proc. Math. Phys. Sci. **434**, 657 (1991).
[159] W. G. C. Boyd, Proc. R. Soc. A **440**, 493 (1993).
[160] W. G. C. Boyd, Proc. R. Soc. A **447**, 609 (1994).
[161] O. Costin and G. V. Dunne, arXiv:2009.01962 [math.CV] [Search INSPIRE].
[162] A. Sen, J. High Energy Phys. **1311**, 029 (2013) [arXiv:1304.0458 [hep-th]] [Search INSPIRE].
[163] C. Beem, L. Rastelli, A. Sen, and B. C. van Rees, J. High Energy Phys. **1404**, 122 (2014) [arXiv:1306.3228 [hep-th]] [Search INSPIRE].
[164] L. F. Alday and A. Bissi, J. High Energy Phys. **1407**, 007 (2014) [arXiv:1311.3215 [hep-th]] [Search INSPIRE].
[165] M. Honda, J. High Energy Phys. **1412**, 019 (2014) [arXiv:1408.2960 [hep-th]] [Search INSPIRE].
[166] M. Honda and D. P. Jatkar, Nucl. Phys. B **900**, 533 (2015) [arXiv:1504.02276 [hep-th]] [Search INSPIRE].
[167] A. Chowdhury, M. Honda, and S. Thakur, J. High Energy Phys. **1704**, 137 (2017) [arXiv:1607.01716 [hep-th]] [Search INSPIRE].
[168] C. Cordova, D. S. Freed, H. T. Lam, and N. Seiberg, SciPost Phys. **8**, 001 (2020) [arXiv:1905.09315 [hep-th]] [Search INSPIRE].
[169] C. Cordova, D. S. Freed, H. T. Lam, and N. Seiberg, SciPost Phys. **8**, 002 (2020) [arXiv:1905.13361 [hep-th]] [Search INSPIRE].
[170] R. Kuik, PhD thesis, Rijksuniversiteit Groningen (2003).